American Mineralogist, Volume 92, pages 532–545, 2007

Co^{2+}-Cu^{2+} substitution in bieberite solid-solution series, $(Co_{1-x}Cu_x)SO_4 \cdot 7H_2O$, $0.00 \leq x \leq 0.46$: Synthesis, single-crystal structure analysis, and optical spectroscopy

Günther J. Redhammer,[1,2,*] Lisa Koll,[1] Manfred Bernroider,[1] Gerold Tippelt,[1] Georg Amthauer,[1] and Georg Roth[2]

[1]Division of Mineralogy, Department of Material Science, University of Salzburg, Hellbrunnerstr. 34, A-5020 Salzburg, Austria
[2]Institute of Crystallography, RWTH—Aachen University, Jägerstr. 17/19, D-52056 Aachen, Germany

Abstract

Single crystals of Cu-substituted bieberite $(Co_{1-x}Cu_x)SO_4 \cdot 7\,H_2O$ have been synthesized from aqueous solution by the evaporation method. It is shown that the solubility of Cu^{2+} in bieberite is limited to 0.46 atoms per formula unit (apfu). Chalcantite $CuSO_4 \cdot 5H_2O$ only accommodates a very small amount of ~0.03 Co^{2+} atoms. Structure analysis by X-ray diffraction of single crystals along the join $CoSO_4 \cdot 7H_2O$–$CuSO_4 \cdot 5H_2O$ showed that the hepta-hydrate phases are monoclinic with $P2_1/c$ symmetry at room temperature, whereas the penta-hydrate phases are triclinic, $P\bar{1}$. Within the $Co_{1-x}Cu_xSO_4 \cdot 7H_2O$ series ($0 \leq x \leq 0.46$), lattice parameters are distinctly altered by the Cu^{2+} substitution, however, the observed changes cannot be ascribed to different ionic radii of Co^{2+} and Cu^{2+} but are due to an increasing distortion of the lattice by increasing Cu^{2+} content. Cu^{2+} is not distributed randomly over the two possible crystallographic metal sites but exclusively enters the M2 site. While all the oxygen atoms coordinating the M1 site act as donors of hydrogen bonding to the sulfate tetrahedron, one oxygen atom at the M2 site is a hydrogen bond acceptor. This may cause the slight tetragonal elongation of the M2 coordination polyhedron, which favors the preferential occupation of this site by Cu^{2+}. Optical spectra show typical features of both the Co^{2+} and the Cu^{2+} absorption signatures. While in Co^{2+}-rich hepta-hydrate phases Co^{2+} absorption bands arising from both M1 and M2 sites are detected, there are only bands arising from the M1 site in $Co_{0.54}Cu_{0.46}SO_4 \cdot 7H_2O$. This supports the observation of selective substitution of Cu^{2+} at the elongated M2 octahedral site. Cu^{2+} absorption bands can be assigned on the basis of D_{4h} symmetry with increasing splitting of the Cu^{2+}, $^2T_{2g}$, and ^2E_g energy levels with increasing Cu^{2+} content.

Keywords: Bieberite, crystal structure, optical spectroscopy, metal sulfate, synthesis

Introduction

Metal sulfates are commonly occurring minerals in mine drainage systems and are also found within the alteration zone of primary sulfides. Among others, chalcantite $CuSO_4 \cdot 5H_2O$ is well known as weathering product of Cu-bearing sulfide minerals. The mineral crystallizes in the triclinic space group P–1 (Bacon and Titterton 1975) and is stable in a relative humidity range from 33 to 97% at 25 °C (Collins and Menzies 1936). In the laboratory large crystals can easily be synthesized from aqueous solution by evaporation of the solvent. Chalcantite is classified as a sulfate mineral with chains of SO_4 tetrahedra and MO_6 octahedra (Hawthorne et al. 2000). The hepta-hydrate bieberite, $CoSO_4 \cdot 7H_2O$ is monoclinic, with space group $P2_1/c$ (Kellerson et al. 1991). It is isostructural with melanterite $FeSO_4 \cdot 7H_2O$ (Baur 1964a), alpersite $(Mg,Cu)SO_4 \cdot 7H_2O$ (Peterson et al. 2006), and mallardite $MnSO_4 \cdot 7H_2O$. Zinc-melanterite $ZnSO_4 \cdot 7H_2O$ and boothite $CuSO_4 \cdot 7H_2O$ are also regarded to be isostructural with melanterite (Leverett et al. 2004; Hawthorne et al. 2000), however their 3-dimensional structure—as well as the one of mallardite itself—is not yet determined. The hepta-hydrates epsomite $MgSO_4 \cdot 7H_2O$ (Baur 1964b; Calleri et al. 1984), morenosite $NiSO_4 \cdot 7H_2O$ (Iskhakova et al. 1991) and goslarite $ZnSO_4 \cdot 7H_2O$ are orthorhombic and represent a second possible structure type within the hepta-hydrate sulfate minerals. Bieberite is usually described as a synthetic material because the natural mineral occurs very rarely as a secondary alteration product e.g., in Co-mines. Stereo-chemically bieberite belongs to the sulfate minerals with isolated SO_4 tetrahedra and $Co(H_2O)_6$ octahedra (Hawthorne et al. 2000). It is only stable at high humidity conditions and decomposes rapidly when being exposed to ambient conditions (e.g., 25 °C, humidity below 70%, Waller 1992) under which it transforms to $CoSO_4 \cdot 6H_2O$ (moorhouseite).

While the basic features of the bieberite structure are known (Kellerson et al. 1991), there is no information on the solubility of metal cations replacing Co^{2+} along binary solid-solution series. The aim of the present investigation is (1) to study the possible amount of Co^{2+} that can be replaced by Cu^{2+} along the join bieberite–$CuSO_4 \cdot nH_2O$ (n = 5, 7), (2) follow in detail changes in structural and distortional parameters, and (3) to examine possible cationic ordering of Co and Cu on the two crystallographically distinct transition metal sites. In the very recent study of Peterson et al. (2006) on alpersite $(Mg,Cu)SO_4 \cdot 7H_2O$ it was found that Cu^{2+} prefers the M2 site. Optical absorption

* E-mail: guenther.redhammer@sbg.ac.at

spectroscopy is used to further characterize the samples and to detect even small amounts of Cu and Co incorporated into the structure of bieberite and/or chalcantite.

Experimental methods

For syntheses of end-member and solid-solution compounds reagent grade $CuSO_4 \cdot 5H_2O$ and $CoSO_4 \cdot 7H_2O$ were weighted in the stoichiometry of the desired crystal composition. The powdered mixtures of $(Cu,Co)SO_4 \cdot nH_2O$ were dissolved in 100 mL of deionized water to give saturated solutions at room temperature. Single crystals were grown by slow evaporation of the solvent. Temperature was kept constant at 25(2) °C using a climatic chamber. Synthesis of large single crystals (up to 40 mm in diameter) was also performed in a home designed single crystal growth apparatus. To prevent the sample material from rapid dehydration, the crystals were kept either at constant humidity of about 75% using a saturated solution of NaCl or covered with silicon oil.

The chemical composition of the sulfate minerals was determined by electron microprobe analysis. Small pieces of the material were glued on a glass slide, covered with carbon and analyzed with a JEOL JXA 8600 electron microprobe. The acceleration voltage was 15 kV, beam current 40 nA and the beam diameter was defocused to 40 µm. As samples were unstable under the electron beam, a large beam diameter had to be used to prevent rapid decomposition. For analysis CuS, $BaSO_4$, and metallic Co were used as standard materials and a ZAF matrix correction was applied to the count rates obtained. Chemical formulas were calculated on basis of 4 oxygen atoms.

During the selection of suitable single crystals for X-ray diffraction crystal aggregates were covered with silicon oil since Co-rich compositions rapidly dehydrate within a few minutes when being kept at ambient conditions (25 °C, 35% humidity). For diffraction experiments selected crystals were fixed to glass capillaries (outer diameter 0.1 mm, wall thickness 0.01 mm) using nail polish. It turned out that embedding samples with nail polish successfully prevented them from dehydration during data collection times except for pure bieberite end-member. Single-crystal X-ray diffraction was performed using a Bruker SMART APEX CCD-diffractometer. Intensity data were collected in 2400 frames with increasing ω (width of 0.3° in ω at 4 different φ positions) and in 900 frames with increasing φ (width of 0.3° in φ). Lattice parameters were determined from single-crystal X-ray diffraction data. Absorption correction was done empirically via equivalents using the SHAPE software (Stoe and Cie 1996). Structure solution (using Patterson methods) and subsequent refinement was carried out with the programs SHELXS-97 and SHELXL-97 (Sheldrick 1997) as implemented in the program suite WinGX 1.64 (Farrugia 1999). X-ray scattering factors in their ionic form, together with anomalous dispersion coefficients were taken from the *International Tables for Crystallography* (Wilson 1992). The program DIAMOND 3.0 (Brandenburg and Putz 2005) was used to prepare the graphical visualization of the crystal structure.

All polarized absorption spectra were obtained at room temperature with a ZEISS USMP 80 microscope spectral photometer. The step width was 2 nm in the UV-VIS region (35 000–12 500 cm^{-1}) and 8 nm in the NIR-region (12 500–5000 cm^{-1}). In both regions, the average of 20 measurements at one step was taken. A PMT-detector (for UV-VIS) and a PbS-detector (for NIR) were used to gather the raw data. The measuring spot was 40 µm in diameter. Among the investigated sulfates only chalcantite is stable at ambient conditions. Thus for this composition it was possible to prepare crystal slides, embedded in epoxy resin, polished on both sides and oriented perpendicular to the $(1\bar{1}0)$ plane. The investigated crystal had a thickness of 85 µm. The other synthetic sulfates are unstable at ambient humidity and temperature and decompose very rapidly and we did not succeed in preparing oriented double-polished single-crystal slides. Therefore either small crystals or cut pieces of crystals, put onto a glass slide, were used to obtain optical absorption spectra, but even here the crystals are not stable over a long period under the optical light beam and it was not possible to obtain spectra in two orientations for all compositions. Based on the outer morphology, we determined the crystals to be oriented in such a way as that the incident light is perpendicular to the $(1\bar{1}0)$ faces. The program PEAKFIT (Systat Software Inc. 1995) was used for the de-convolution of spectra into Gaussian shaped curves. In light of the fact that the crystals of the hepta-hydrate series were not stable at ambient conditions and thus could not be oriented perfectly, we do not stress the interpretation of our optical absorption spectra. However, the spectra and data presented here are, to our best knowledge, the best and most complete ones given in literature so far and several well-defined trends can be extracted.

Results and discussion

Synthesis and material chemistry

Over a period of several weeks, aggregates of reddish to reddish brown crystals (depending on the Cu content) formed at the bottom of the beaker for compositions of $(Co_{1-x}Cu_x)SO_4 \cdot 7H_2O$ with $0.0 \leq x \leq 0.46$. Individual single crystals were between 2 to 10 mm in size. The crystals show well-developed faces and display a slight pleochroism from pale to a more intense reddish brown color. An experiment with a starting Cu^{2+} content of $x = 0.5$ (Bieb50) yielded two different types of crystals, blue and reddish brown ones. This appearance of two different types of crystals clearly shows the presence of a miscibility gap between Co and Cu sulfate end-members. According to the chemical analyses (Table 1) the solubility of Cu^{2+} in bieberite is limited to 0.46 atoms per formula unit (apfu), whereas chalcantite only accommodates a very limited amount of 0.03 Co^{2+} atoms per formula unit. Within experimental error, the chemical composition of the solid-solution compounds within the bieberite stability field agrees well with the one of the starting composition of the solution and the crystals appear to be homogeneous, i.e., they neither show chemical zoning within nor between crystals.

Structure refinement

The analysis of reflection conditions indicated space group $P2_1/c$ for all red to reddish brown colored solid-solution compounds. Structure solution using Patterson methods revealed metal cation positions. Oxygen atoms were located in subsequent structure refinement cycles; hydrogen positions were determined from difference electron density maps. For pure bieberite, only ten of the twelve protons could be located, one of the H-atoms associated with both O6 and O9 is missing. Probably this is due to the partial dehydration of the sample during data collection. Full matrix least squares refinement on F^2 using anisotropic atomic displacement parameters for all non-H atoms converged to final agreement factors of $R_1 < 3\%$ for all data sets. It follows from space group symmetry and fractional atomic coordinates that the reddish to reddish brown colored solid-solution compounds are isotypic and isostructural with the melanterite structure type, thus representing a hepta-hydrate solid-solution series $(Co_{1-x}Cu_x)SO_4 \cdot 7H_2O$ for $0 \leq x \leq 0.46$. The blue crystals of the experiment Bieb50 are triclinic, space group $P\bar{1}$. Structure solution and subsequent full matrix structure refinement on F^2 showed the chalcantite structure type. Based on electron microprobe analysis and structure determination, the chemical composition of the blue crystals of experiment Bieb50 is $(Co_{0.03}Cu_{0.97})SO_4 \cdot 5H_2O$. Lattice parameters and final fractional atomic coordinates agree well with those given in the references, e.g., Bacon and Titterton (1975). A summary of experimental conditions and results of structure refinement are contained in Table 2a for the hepta-hydrate and in Table 2b[1] for the penta-hydrate compounds; Table 3 gives the fractional atomic coordinates while Table 4 contains selected interatomic distances, angles, and polyhedral distortion parameters. Below, the focus of discussion will be on the structural changes within the hepta-hydrate series with only minor comparisons to the penta-hydrate phases.

TABLE 1. Chemical composition of synthetic compounds of the $CoSO_4$·7H_2O–$CuSO_4$·5H_2O join as determined by electron microprobe analysis

Run	Bieb no. 3	Bieb no. 07	Bieb no. 12	Bieb no. 18	Bieb no. 25	Bieb no. 35	Bieb no. 50_r	Bieb no. 50_b	Calc
n	9	12	11	14	12	15	15	15	15
CoO	39.9(6)	38.8(5)	36.7(5)	34.1(4)	30.9(4)	27.5(4)	22.3(4)	1.3(5)	0
CuO	1.3(5)	3.1(4)	5.3(5)	7.9(5)	11.1(4)	15.2(5)	20.2(4)	44.0(4)	45.2(5)
SO_3	43.0(6)	44.5(6)	44.0(4)	44.9(5)	44.1(4)	44.7(5)	43.7(4)	46.1(4)	44.5(4)
sum	84.2	86.4	85.9	86.9	86.1	87.4	86.1	91.4	90.6
Formula based on 4 oxygen atoms									
Co	0.97	0.94	0.89	0.82	0.74	0.67	0.54	0.03	–
Cu	0.03	0.07	0.12	0.18	0.25	0.35	0.46	0.97	1.00
S	0.98	1.01	1.00	1.01	0.99	1.02	0.99	1.01	1.00

Notes: n = number of single spot analyses merged to average values given in Table; numbers in parenthesis are one standard deviation; _r and _b for sample Bieb#50 denote the red and the blue crystals respectively.

TABLE 2A. Data collection parameters and results of structure refinement for ($Co_{1-x}Cu_x$)SO_4·7H_2O

xCu		0.00	0.03	0.07	0.12	0.18	0.25	0.35	0.46
Space group		$P2_1/c$	$P2_1/c$	$P2_1/c$	$P2_1/c$	$P2_1/c$	$P2_1/c$	$P2_1/c$	$P2_1/c$
Z		4	4	4	4	4	4	4	4
Lattice parameters:	*a* (Å)	14.0362(16)	14.0393(16)	14.0442(12)	14.0474(12)	14.0533(12)	14.0633(12)	14.0715(12)	14.0875(12)
	b (Å)	6.4957(7)	6.4958(7)	6.4966(5)	6.4974(5)	6.4983(5)	6.5024(5)	6.5068(5)	6.5124(5)
	c (Å)	10.9256(12)	10.9187(12)	10.9121(9)	10.9041(9)	10.8904(9)	10.8771(9)	10.8647(9)	10.8397(9)
	β (°)	105.322(1)	105.327(2)	105.349(1)	105.3650(1)	105.384(1)	105.398(1)	105.443(1)	105.509(1)
V (Å^3)		960.73(18)	960.33(18)	960.10(14)	959.66(14)	958.90(14)	958.95(14)	958.86(14)	958.26(14)
Density$_{(calc)}$ (mg/cm^3)		1.954	1.946	1.946	1.947	1.949	1.949	1.949	1.950
Crystal size (mm^3)		0.32 x 0.26 x 0.17	0.25 x 0.20 x 0.18	0.23 x 0.21 x 0.16	0.19 x 0.16 x 0.15	0.20 x 0.18 x 0.15	0.18 x 0.15 x0.12	0.21 x 0.18 x 0.15	0.17 x 0.15 x 0.10
Crystal color		red	red	red	red	red–brown	red–brown	red–brown	red–brown
θ range data collection (°)		1.50–28.21	3.01–28.27	3.01–28.26	1.50–28.74	1.50–28.89	1.50–28.71	1.50–28.82	1.50–28.78
Index range:	*h*	–18 ... 18	–18 ... 18	–18 ... 18	–18 ... 14	–19 ... 18	–18 ... 18	–18 ... 18	–19 ... 18
	k	–1 ... 8	–8 ... 8	–8 ... 8	–7 ... 8	–8 ... 8	–8 ... 8	–8 ... 8	–8 ... 8
	l	–12 ... 11	–14 ... 14	–14 ... 14	–12 ... 12	–14 ... 14	–14 ... 14	–14 ... 14	–14 ... 14
Reflections collected		2866	13626	12935	8659	11979	13205	10882	11348
Independent reflections		1800	2344	2348	1900	2397	2381	2374	2367
R_{int} (%)		5.37	5.52	3.76	3.61	4.93	2.97	6.78	3.52
Completeness of data (%)		75.6	98.1	98.3	76.3	95.3	95.9	94.9	94.8
No. of parameters		170	178	177	178	177	177	177	177
R_1 index [$I > 2\sigma$] (%)		5.06	2.30	2.44	2.24	2.47	2.36	2.63	2.32
R_1 all data (%)		5.65	2.52	2.87	2.67	3.33	2.67	2.88	2.61
wR_2 index [$I > 2\sigma$] (%)		11.39	6.14	6.52	5.87	5.85	6.30	6.42	6.08
wR_2 all data (%)		11.76	6.27	6.68	6.02	6.10	6.43	5.58	6.23
Goodness-of-fit on F^2		1.094	1.054	1.007	1.035	0.955	1.047	1.045	1.038
Extinction coefficient		0.0038	0.0048(7)	–	0.0030(7)	–	–	–	–
Largest diff. peak (e Å^{-3})		1.477	0.311	0.310	0.239	0.306	0.356	0.309	0.378
Largest diff. hole (e Å^{-3})		–1.111	–0.403	–0.427	–0.377	–0.343	–0.415	–0.477	–0.379

Lattice parameters

All lattice parameters were determined from single-crystal X-ray diffraction data (Table 2). Though the ionic radius of both metal cations is similar ($^{[VI]}Co^{2+}$ = 0.735 Å, $^{[VI]}Cu^{2+}$ = 0.730 Å, Shannon and Prewitt 1969) the substitution of Co^{2+} by Cu^{2+} distinctly alters the lattice parameters within the bieberite solid-solution series. Most prominent is the decrease of the *c* lattice parameter (Fig. 1c), while *a*, *b,* and the monoclinic angle β increase with increasing Cu^{2+} content (Figs. 1a, 1b, and 1d). Compared to the unit-cell parameters of the pure Co^{2+} end-member, the largest relative change upon the substitution of Co^{2+} by Cu^{2+} is observed for the *c* lattice parameter, while the other changes are smaller (Fig. 1e). The variation of the unit-cell volume is dominated by the large decrease of the *c* lattice parameter.

Structural topology of the ($Co_{1-x}Cu_x$)SO_4·7H_2O series

The structure of bieberite consists of two types of crystallographic distinct and isolated octahedra M1 and M2, which are fully hydrated giving two $[Co^{2+}(H_2O)_6]^{2+}$ units arranged in a pseudo face-centered lattice. In addition, the structure contains an isolated sulfate tetrahedron $[SO_4]^{2-}$ and a single isolated water molecule. These four components of the structure are connected to each other by hydrogen bonds. The general structural topology of bieberite is displayed in Figure 2. The structural parameters of bieberite found in this study agree well with those given in Kellerson et al. (1991) for $CoSO_4$·7D_2O and also compare well with the data for melanterite (Baur 1964a) and alpersite (Peterson et al. 2006).

The two Co^{2+} atoms are located at an inversion center ($\bar{1}$ symmetry). The M1 polyhedron has four long and two short Co^{2+}-O bond lengths leading to a tetragonally compressed M1-octahedron (Table 4). In terms of polyhedral distortion parameters the M1 site shows only small deviations from ideal

[1] Deposit item AM-07-014, Table 2b (experimental conditions and results of structure refinement for the penta-hydrate compounds). Deposit items are available two ways: For a paper copy contact the Business Office of the Mineralogical Society of America (see inside front cover of recent issue) for price information. For an electronic copy visit the MSA web site at http://www.minsocam.org, go to the American Mineralogist Contents, find the table of contents for the specific volume/issue wanted, and then click on the deposit link there.

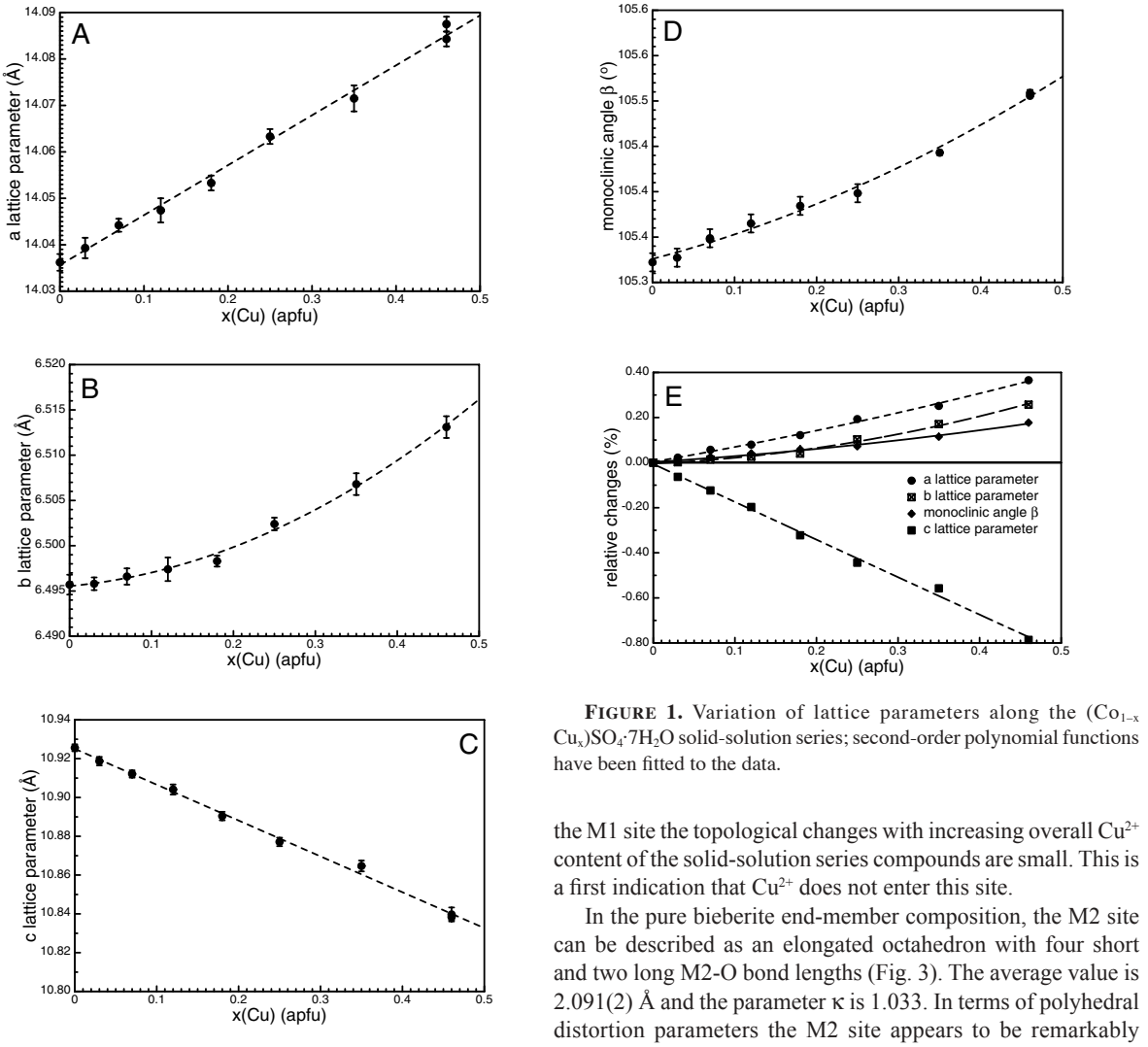

FIGURE 1. Variation of lattice parameters along the $(Co_{1-x}Cu_x)SO_4·7H_2O$ solid-solution series; second-order polynomial functions have been fitted to the data.

octahedral geometry (Table 4). The substitution of Co^{2+} by Cu^{2+} in the $(Co_{1-x}Cu_x)SO_4·7H_2O$ series ($0 \le x \le 0.46$) only slightly alters the individual M1-O bond lengths . The M1-O11 bond length increases by 0.58% while the M1-O7 and M1-O8 bonds shorten by 0.25 and 0.77%, respectively; on average, however, the <M1-O> bond lengths remain almost constant (decreases by 0.14%). Among the polyhedral distortion parameters, the bond length distortion (BLD) slightly increases; the edge length distortion (ELD) and the quadratic octahedral elongation (QOE) remain constant while the octahedral angle variance (OAV) decreases. The value κ [$\kappa = <M\text{-}O>_{ap}/<M\text{-}O>_{eq}$ ($<M\text{-}O>_{ap}$ = the average M-O bond lengths from the central octahedral cation to the apex oxygen atoms and $<M\text{-}O>_{eq}$ = the average of the M-O bond lengths within the equatorial plane of an octahedron)] can be used as a measure of (tetragonal) compression ($\kappa < 1$) or elongation ($\kappa > 1$). For the M1 site in bieberite $\kappa = 0.964$ and decreases by about 1% toward the Cu-richest member of the solid-solution series. The value of κ of M1 in bieberite compares well with those in melanterite ($\kappa = 0.966$, Baur 1964a) and alpersite ($\kappa = 0.966$ and 0.974 for the data given by Peterson et al. 2006). Generally at the M1 site the topological changes with increasing overall Cu^{2+} content of the solid-solution series compounds are small. This is a first indication that Cu^{2+} does not enter this site.

In the pure bieberite end-member composition, the M2 site can be described as an elongated octahedron with four short and two long M2-O bond lengths (Fig. 3). The average value is 2.091(2) Å and the parameter κ is 1.033. In terms of polyhedral distortion parameters the M2 site appears to be remarkably regular as shown by the very small OAV and QOE parameters (Table 4). Only the edge length distortion—still small—is slightly larger at the M2 site compared to M1. While the average M2-O bond length increases by merely 0.45% (0.01 Å) from $CoSO_4·7H_2O$ to $(Co_{0.54}Cu_{0.46})SO_4·7H_2O$, very pronounced changes among the individual M2-O bond lengths (Fig. 3) are observed. With increasing total Cu^{2+} content of the samples the 4 short equatorial M2-O bonds decrease by 2.84% and 3.54% for the M2-O5 and M2-O6 bond, respectively, and are almost the same length as those in the most Cu^{2+}-enriched hepta-hydrate phase. In contrast, the two long bonds in bieberite increase by as much as 7.5% [corresponding to 0.160(2) Å]. The bond lengths at M2 in alpersite (with the M2 site filled by ~80% Cu^{2+}) are similar to those found here, namely 1.994(4)–2.028(3) Å for the four short bonds and 2.302(3)–2.328(4) Å for the two long bonds in the two different samples investigated by Peterson et al. (2006). This indicates a similar chemical composition of the M2 site in Cu^{2+}-rich bieberite and alpersite. In investigating the geometry of 159 symmetrically unique (4+2)-distorted $Cu^{2+}O_6$ octahedra in 90 different Cu^{2+} oxysalt minerals, Burns and Hawthorne (1996) state that the average $<Cu^{2+}\text{-}O_{eq}>$ is 1.973

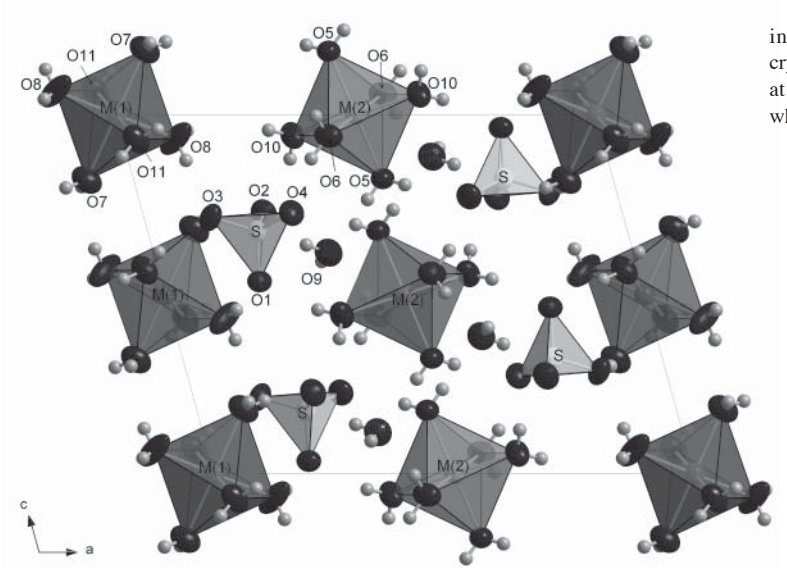

FIGURE 2. Structure of $(Co_{0.97}Cu_{0.03})SO_4·7H_2O$ in polyhedral representation in a view along the crystallographic *b* axis. The thermal ellipsoids are drawn at the 80% probability level except hydrogen atoms, which are drawn with an arbitrary radius.

Å with a standard deviation of 0.048 Å, while the <Cu^{2+}-O_{ap}> distance is 2.505 Å with a standard deviation of 0.205 Å. The data for the most Cu-rich bieberite and the ones for alpersite fit these average values almost perfectly for the <Cu^{2+}-O_{eq}> and are within the range of expectable values for <Cu^{2+}-O_{ap}>. This is seen as a further evidence that Cu^{2+} enters the M2 site within the $(Co_{1-x}Cu_x)SO_4·7H_2O$ series. Furthermore, it is interesting to note that extrapolation of the data of the $(Co_{1-x}Cu_x)SO_4·7H_2O$ series toward x = 0.97 and 1.00 leads to individual Cu^{2+}-O bond lengths, which are very similar to those found for the M2 site in pure $CuSO_4·5H_2O$ and $Co_{0.03}Cu_{0.97}SO_4·5H_2O$ in this study (Fig. 3). It is the M2 site, which shows a larger polyhedral distortion in the chalcantite structure as compared to the M1 site (Table 4b). Furthermore, given the replacement of only 0.03 Cu^{2+} by Co^{2+}, the changes of the individual M1 bond lengths are actually quite large with a shortening of the two long bonds by 0.010(1) Å and an increase of the four short bonds by 0.005(1) Å. These changes may be indicative of a preferred Co^{2+} incorporation onto this site in the chalcantite structure.

The fact that there are only minor changes on the M1 site in bieberite, but very pronounced bond length changes with the beginning of the formation of a fourfold planar coordination around the M2 site is seen as a strong evidence that incorporation of Cu^{2+} almost exclusively takes place at the M2 site in the bieberite structure. Furthermore, the observed strong distortion of the M2 site in Cu-rich bieberite (and in alpersite) can be ascribed to the strong Jahn-Teller distortion of Cu^{2+}. The Jahn-Teller theorem states that transition metal cations having a degenerate electronic state related to partially filled d-orbitals (such as d^9 in Cu^{2+}) distort to a system with lower symmetry, thereby partly removing the degeneracy (e.g., Benabbas 2006; Burns and Hawthorne 1996). For octahedra the degeneracy is generally removed by a tetragonal elongation of octahedra while the inverse case (tetragonal compression) rarely was observed. Substitution of Cu^{2+} at M2 thus causes a strong distortion of the coordination of the M2 site. Indeed, this is observed: the M2 site becomes more elongated and the coordination changes from 6 to 4+2 (increasing value

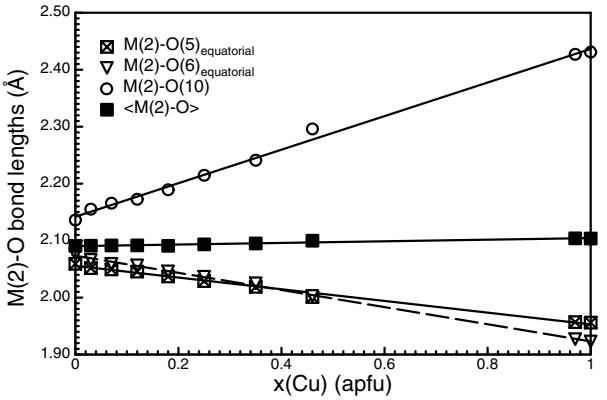

FIGURE 3. Variation of individual and average bond lengths for the M2 site along the $(Co_{1-x}Cu_x)SO_4·7H_2O$ solid-solution series including an extrapolation of the M2 site data toward $CuSO_4·5H_2O$; linear regression lines have been fitted to the data.

of κ, Fig. 4a), while there is almost no change in the tetragonal compression of the coordination octahedron around the M1 site. Compressed M1 sites as also found in melanterite and alpersite appear to be highly "unattractive" for Cu^{2+} substitution from the crystal chemical point of view. It can be concluded that the limited solubility of Cu^{2+} in bieberite is a consequence of rejection of Cu^{2+} at the tetragonally compressed M1 site.

As a consequence of the pronounced bond length changes on M2, the bond length distortion BLD and the edge length distortion ELD increase distinctly with increasing Cu^{2+} content of the samples (Figs. 4b and 4c, respectively). While the ELD is lower for the M2 than for the M1 site in Cu^{2+}-poor samples, it is higher in the Cu^{2+}-rich members of the solid-solution series. A behavior very similar to the ELD on M1 and M2 is observed for the quadratic octahedral elongation QOE. It is interesting to note that for both the M1 and the M2 sites the octahedral angle variance slightly decreases meaning that the angular distortion decreases with increasing Cu^{2+} content.

TABLE 3. Atomic positional parameters and equivalent isotropic displacement parameters for the synthetic compounds of the $Co_{1-x}Cu_xSO_4 \cdot nH_2O$ series with n = 7 for x ≤ 0.46 (bieberite series) and n = 5 for x = 0.97 and 1.00 (chalcantite series)

	x	y	z	U(eq)
x = 0.00*				
M(1)	0	0	0	0.0238(2)
M(2)	½	½	0	0.0235(2)
S(1)	0.2268(1)	0.4724(1)	0.1766(1)	0.0227(2)
O(1)	0.2045(1)	0.4706(3)	0.364(1)	0.0306(6)
O(2)	0.2521(1)	0.2634(2)	0.2261(2)	0.0336(5)
O(3)	0.1383(2)	0.5431(3)	0.2140(2)	0.0341(5)
O(4)	0.3092(1)	0.6127(3)	0.2271(2)	0.0345(5)
O(5)	0.5199(2)	0.5491(4)	−0.1778(2)	0.0326(6)
O(6)	0.4314(2)	0.2200(3)	−0.0578(3)	0.0367(6)
O(7)	−0.0977(1)	0.0382(4)	−0.1812(1)	0.0398(6)
O(8)	0.1110(1)	0.1149(4)	−0.0674(2)	0.0551(6)
O(9)	0.3637(2)	0.0051(3)	0.1170(3)	0.0371(6)
O(10)	0.3577(2)	0.6410(3)	−0.0581(3)	0.0360(6)
O(11)	0.0285(2)	−0.2917(2)	−0.0681(2)	0.0365(6)
H(5a)	0.466(3)	0.550(6)	−0.244(5)	0.047(11)
H(5b)	0.570(3)	0.526(6)	−0.175(5)	0.048(12)
H(6b)	0.384(3)	0.225(7)	−0.127(5)	0.066(15)
H(7a)	−0.153(4)	−0.050(8)	−0.208(6)	0.097(18)
H(7b)	−0.113(4)	0.145(8)	−0.199(5)	0.083(17)
H(8a)	0.142(3)	0.179(6)	−0.052(4)	0.045(11)
H(8b)	0.401(4)	0.193(9)	−0.020(6)	0.100(21)
H(9b)	0.335(4)	−0.064(8)	0.091(6)	0.082(19)
H(10a)	0.312(3)	0.598(6)	−0.042(4)	0.040(10)
H(10b)	0.345(3)	0.705(6)	−0.119(4)	0.050(12)
H(11a)	0.070(3)	−0.356(6)	−0.051(4)	0.047(11)
H(11b)	−0.022(4)	−0.388(7)	−0.117(5)	0.091(15)
x = 0.03				
Co	0	0	0	0.02437(6)
Cu	½	½	0	0.02408(6)
S(1)	0.2270(1)	0.4717(1)	0.1765(1)	0.02296(7)
O(1)	0.2044(1)	0.4703(1)	0.362(1)	0.0322(2)
O(2)	0.2525(1)	0.2625(1)	0.2266(1)	0.0346(2)
O(3)	0.1389(1)	0.5426(2)	0.2142(1)	0.0353(2)
O(4)	0.3102(1)	0.6112(2)	0.2267(1)	0.0362(2)
O(5)	0.5198(1)	0.5498(2)	−0.1772(1)	0.0341(2)
O(6)	0.4314(1)	0.2221(1)	−0.0584(1)	0.0368(2)
O(7)	−0.0977(1)	0.0388(2)	−0.1813(1)	0.0401(2)
O(8)	0.1116(1)	0.1145(2)	−0.0661(1)	0.0568(3)
O(9)	0.3649(1)	0.0055(2)	0.1163(1)	0.0375(2)
O(10)	0.3567(1)	0.6438(2)	−0.0575(1)	0.0386(2)
O(11)	0.0288(1)	−0.2920(2)	−0.0679(1)	0.0369(2)
H(5a)	0.4764(17)	0.533(3)	−0.236(2)	0.050(6)
H(5b)	0.5627(15)	0.498(2)	−0.194(2)	0.038(5)
H(6a)	0.4158(17)	0.157(3)	−0.005(2)	0.070(7)
H(6b)	0.3823(18)	0.222(3)	−0.122(2)	0.076(7)
H(7a)	−0.1458(16)	−0.033(3)	−0.203(2)	0.055(6)
H(7b)	−0.1123(15)	0.156(3)	−0.2001(18)	0.054(6)
H(8a)	0.1203(15)	0.072(3)	−0.127(2)	0.057(6)
H(8b)	0.1399(15)	0.215(3)	−0.0436(19)	0.057(6)
H(9a)	0.3229(18)	0.069(4)	0.138(2)	0.071(7)
H(9b)	0.3455(16)	−0.105(4)	0.092(2)	0.068(7)
H(10a)	0.3097(15)	0.582(3)	−0.0428(18)	0.052(5)
H(10b)	0.3382(15)	0.711(3)	−0.123(2)	0.058(6)
H(11a)	0.0784(14)	−0.360(3)	−0.0409(16)	0.045(5)
H(11b)	−0.0111(18)	−0.362(3)	−0.117(2)	0.071(7)
x = 0.07				
Co	0	0	0	0.0240(1)
Cu	½	½	0	0.0239(1)
S(1)	0.2271(1)	0.4715(1)	0.1766(1)	0.0228(1)
O(1)	0.2044(1)	0.4701(2)	0.0363(1)	0.0319(2)
O(2)	0.2524(1)	0.2622(2)	0.2264(1)	0.0342(3)
O(3)	0.1392(1)	0.5428(2)	0.2144(1)	0.0350(3)
O(4)	0.3103(1)	0.6108(2)	0.2266(1)	0.0359(3)
O(5)	0.5198(1)	0.5497(2)	−0.1770(1)	0.0336(3)
O(6)	0.4315(1)	0.2233(2)	−0.0583(1)	0.0366(3)
O(7)	−0.0977(1)	0.0392(2)	−0.1813(1)	0.0402(3)
O(8)	0.1115(1)	0.1145(2)	−0.0660(2)	0.0566(4)
O(9)	0.3650(1)	0.0058(2)	0.1161(1)	0.0370(3)
O(10)	0.3561(1)	0.6447(2)	−0.0575(1)	0.0387(3)
O(11)	0.0289(1)	−0.2920(2)	−0.0680(1)	0.0369(3)
H(5a)	0.4754(19)	0.536(3)	−0.235(2)	0.047(6)
H(5b)	0.5670(20)	0.495(3)	−0.189(3)	0.053(7)
H(6a)	0.4181(18)	0.165(4)	−0.006(2)	0.060(7)
H(6b)	0.3830(20)	0.217(4)	−0.121(3)	0.079(8)
H(7a)	−0.1455(18)	−0.038(4)	−0.207(2)	0.058(7)
H(7b)	−0.1143(16)	0.156(4)	−0.198(2)	0.054(6)
H(8a)	0.1174(16)	0.078(4)	−0.129(2)	0.052(6)
H(8b)	0.1397(17)	0.215(4)	−0.044(2)	0.054(6)
H(9a)	0.3200(20)	0.066(4)	0.137(3)	0.076(8)
H(9b)	0.3451(18)	−0.095(4)	0.095(2)	0.068(8)
H(10a)	0.3066(19)	0.590(4)	−0.043(2)	0.068(7)
H(10b)	0.3389(18)	0.717(4)	−0.123(2)	0.072(7)
H(11a)	0.0789(16)	−0.364(3)	−0.0412(18)	0.045(5)
H(11b)	−0.0121(19)	−0.364(3)	−0.115(2)	0.069(7)
x = 0.12				
Co	0	0	0	0.0244(1)
Cu	½	½	0	0.0246(1)
S(1)	0.2271(1)	0.4714(1)	0.1766(1)	0.0238(1)
O(1)	0.2044(1)	0.4700(2)	0.0364(1)	0.0329(3)
O(2)	0.2523(1)	0.2622(1)	0.2263(1)	0.0354(3)
O(3)	0.1392(1)	0.5429(2)	0.2143(1)	0.0362(3)
O(4)	0.3102(1)	0.6107(2)	0.2267(1)	0.0375(3)
O(5)	0.5198(1)	0.5496(2)	−0.1768(1)	0.0346(3)
O(6)	0.4316(1)	0.2236(2)	−0.0583(2)	0.0379(3)
O(7)	−0.0976(1)	0.0393(2)	−0.1812(1)	0.0414(4)
O(8)	0.1113(1)	0.1147(3)	−0.0659(2)	0.0577(5)
O(9)	0.3652(1)	0.0060(2)	0.1161(2)	0.0382(3)
O(10)	0.3557(1)	0.6453(2)	−0.0577(1)	0.0400(3)
O(11)	0.0289(1)	−0.2919(2)	−0.0680(1)	0.0380(3)
H(5a)	0.474(2)	0.534(3)	−0.234(3)	0.054(8)
H(5b)	0.569(2)	0.503(3)	−0.188(3)	0.053(8)
H(6a)	0.4158(17)	0.161(4)	−0.008(2)	0.056(8)
H(6b)	0.385(2)	0.223(3)	−0.116(2)	0.065(8)
H(7a)	−0.1409(19)	−0.036(4)	−0.203(2)	0.062(8)
H(7b)	−0.1131(17)	0.159(4)	−0.200(2)	0.065(8)
H(8a)	0.1174(16)	0.079(4)	−0.128(2)	0.053(7)
H(8b)	0.1413(17)	0.213(4)	−0.044(2)	0.057(7)
H(9a)	0.322(2)	0.064(4)	0.137(3)	0.074(9)
H(9b)	0.3460(18)	−0.097(4)	0.093(2)	0.070(9)
H(10a)	0.3058(18)	0.584(4)	−0.045(2)	0.059(6)
H(10b)	0.3413(19)	0.711(4)	−0.124(2)	0.074(8)
H(11a)	0.0787(16)	−0.359(3)	−0.0413(19)	0.046(6)
H(11b)	−0.0109(19)	−0.361(4)	−0.114(2)	0.065(8)
x = 0.18				
Co	0	0	0	0.0245(1)
Cu	½	½	0	0.0247(1)
S(1)	0.2273(1)	0.4706(1)	0.1764(1)	0.0239(1)
O(1)	0.2040(1)	0.4692(2)	0.0359(1)	0.0329(3)
O(2)	0.2523(1)	0.2613(2)	0.2263(1)	0.0354(3)
O(3)	0.1398(1)	0.5429(2)	0.2148(1)	0.0366(3)
O(4)	0.3108(1)	0.6092(2)	0.2262(1)	0.0369(3)
O(5)	0.5196(1)	0.5502(2)	−0.1763(1)	0.0349(3)
O(6)	0.4316(1)	0.2256(2)	−0.0587(2)	0.0383(3)
O(7)	−0.0977(1)	0.0392(2)	−0.1813(1)	0.0417(3)
O(8)	0.1112(1)	0.1141(3)	−0.0662(2)	0.0584(5)
O(9)	0.3660(1)	0.0064(2)	0.1156(2)	0.0387(3)
O(10)	0.3549(1)	0.6477(2)	−0.0575(1)	0.0416(3)
O(11)	0.0288(1)	−0.2926(2)	−0.0682(1)	0.0380(3)
H(5a)	0.4770(17)	0.535(3)	−0.233(2)	0.040(6)
H(5b)	0.5670(19)	0.499(3)	−0.1890(2)	0.047(7)
H(6a)	0.4173(17)	0.166(4)	−0.010(2)	0.060(8)
H(6b)	0.3840(20)	0.222(4)	−0.118(3)	0.071(9)
H(7a)	−0.1500(20)	−0.036(4)	−0.207(3)	0.075(9)
H(7b)	−0.1125(17)	0.156(4)	−0.1980(2)	0.058(7)
H(8a)	0.1174(15)	0.075(4)	−0.128(2)	0.045(6)
H(8b)	0.1412(16)	0.208(4)	−0.041(2)	0.048(7)
H(9a)	0.3270(19)	0.064(4)	0.133(3)	0.066(9)

* Hydrogen atoms associated with O6 and O9 were not located.

continued on next page

TABLE 3. —*Continued*

	x	y	z	U(eq)
H(9b)	0.3476(18)	–0.099(4)	0.091(2)	0.070(9)
H(10a)	0.3074(16)	0.588(4)	–0.043(2)	0.051(6)
H(10b)	0.3397(17)	0.712(4)	–0.123(2)	0.062(8)
H(11a)	0.0804(17)	–0.368(4)	–0.038(2)	0.059(7)
H(11b)	–0.0096(19)	–0.356(4)	–0.116(3)	0.077(9)
x = 0.25				
Co	0	0	0	0.0251(1)
Cu	½	½	0	0.0248(1)
S(1)	0.2274(1)	0.4698(1)	0.1763(1)	0.0240(1)
O(1)	0.2035(1)	0.4685(2)	0.0354(1)	0.0333(2)
O(2)	0.2522(1)	0.2603(2)	0.2261(1)	0.0355(2)
O(3)	0.1403(1)	0.5427(2)	0.2152(1)	0.0371(3)
O(4)	0.3113(1)	0.6080(2)	0.2256(1)	0.0376(3)
O(5)	0.5193(1)	0.5505(2)	–0.1759(1)	0.0346(3)
O(6)	0.4314(1)	0.2276(2)	–0.0587(1)	0.0379(3)
O(7)	–0.0979(1)	0.0398(2)	–0.1815(1)	0.0416(3)
O(8)	0.1112(1)	0.1138(2)	–0.0660(2)	0.0589(4)
O(9)	0.3666(1)	0.0071(2)	0.1156(1)	0.0382(3)
O(10)	0.3536(1)	0.6508(2)	–0.0571(1)	0.0422(3)
O(11)	0.0284(1)	–0.2923(2)	–0.0684(1)	0.0383(3)
H(5a)	0.4745(19)	0.535(3)	–0.234(3)	0.052(7)
H(5b)	0.5648(19)	0.498(3)	–0.189(2)	0.048(7)
H(6a)	0.4150(17)	0.166(4)	–0.004(2)	0.062(7)
H(6b)	0.388(2)	0.226(4)	–0.118(2)	0.066(7)
H(7a)	–0.1461(19)	–0.037(4)	–0.207(2)	0.062(7)
H(7b)	–0.1145(16)	0.155(4)	–0.197(2)	0.053(6)
H(8a)	0.1159(16)	0.076(4)	–0.130(2)	0.053(6)
H(8b)	0.1404(17)	0.214(4)	–0.043(2)	0.056(6)
H(9a)	0.322(2)	0.069(4)	0.135(2)	0.068(7)
H(9b)	0.3484(18)	–0.094(4)	0.089(2)	0.068(8)
H(10a)	0.3068(18)	0.582(4)	–0.042(2)	0.060(6)
H(10b)	0.3363(18)	0.712(4)	–0.124(2)	0.066(7)
H(11a)	0.0777(16)	–0.365(3)	–0.0406(19)	0.049(6)
H(11b)	–0.009(2)	–0.360(4)	–0.119(2)	0.073(8)
x = 0.35				
Co	0	0	0	0.0256(1)
Cu	½	½	0	0.0253(1)
S(1)	0.2276(1)	0.4686(1)	0.1764(1)	0.0247(1)
O(1)	0.2033(1)	0.4668(2)	0.0355(1)	0.0343(3)
O(2)	0.2522(1)	0.2591(2)	0.2262(1)	0.0345(3)
O(3)	0.1410(1)	0.5428(2)	0.2157(1)	0.0385(3)
O(4)	0.3118(1)	0.6059(2)	0.2253(1)	0.0386(3)
O(5)	0.5192(1)	0.5506(2)	–0.1751(1)	0.0351(3)
O(6)	0.4314(1)	0.2299(2)	–0.0589(1)	0.0387(3)
O(7)	–0.0977(1)	0.0402(2)	–0.1814(1)	0.0428(3)
O(8)	0.1108(1)	0.1130(3)	–0.0660(2)	0.0604(5)
O(9)	0.3674(1)	0.0077(2)	0.1152(1)	0.039(1)
O(10)	0.3523(1)	0.6541(2)	–0.0567(1)	0.0044(1)
O(11)	0.0284(1)	–0.2930(2)	–0.0688(1)	0.0040(1)
H(5a)	0.4772(19)	0.536(3)	–0.234(2)	0.048(7)
H(5b)	0.570(2)	0.498(3)	–0.186(2)	0.047(6)
H(6a)	0.4171(17)	0.174(4)	–0.008(2)	0.057(7)
H(6b)	0.387(2)	0.229(4)	–0.117(3)	0.075(8)
H(7a)	–0.148(2)	–0.035(4)	–0.208(3)	0.074(8)
H(7b)	–0.1148(18)	0.159(4)	–0.196(2)	0.063(7)
H(8a)	0.1164(17)	0.073(4)	–0.131(2)	0.054(6)
H(8b)	0.1409(17)	0.211(4)	–0.043(2)	0.053(6)
H(9a)	0.324(2)	0.060(4)	0.132(3)	0.070(8)
H(9b)	0.3493(18)	–0.091(4)	0.086(2)	0.059(8)
H(10a)	0.3042(18)	0.593(4)	–0.045(2)	0.056(6)
H(10b)	0.3355(18)	0.712(4)	–0.124(2)	0.067(7)
H(11a)	0.0789(17)	–0.366(3)	–0.0427(19)	0.049(6)
H(11b)	–0.010(2)	–0.364(4)	–0.118(3)	0.082(9)
x = 0.46				
Co	0	0	0	0.0254(1)
Cu	½	½	0	0.0246(1)
S(1)	0.2281(1)	0.4670(1)	0.1758(1)	0.0244(1)
O(1)	0.2025(1)	0.4655(2)	0.0344(1)	0.0339(2)
O(2)	0.2521(1)	0.2572(2)	0.2257(1)	0.0359(3)
O(3)	0.1425(1)	0.5429(2)	0.2166(1)	0.0387(3)
O(4)	0.3129(1)	0.6028(2)	0.2243(1)	0.0382(3)
O(5)	0.5189(1)	0.5515(2)	–0.1739(1)	0.0339(3)
O(6)	0.4312(1)	0.2345(2)	–0.0595(1)	0.0377(3)
O(7)	–0.0982(1)	0.0411(2)	–0.1816(1)	0.0430(3)
O(8)	0.1103(1)	0.1125(3)	–0.0665(2)	0.0612(5)
O(9)	0.3686(1)	0.0090(2)	0.1142(1)	0.0375(3)
O(10)	0.3495(1)	0.6606(2)	–0.0566(1)	0.0426(3)
O(11)	0.0280(1)	–0.2928(2)	–0.0692(1)	0.0396(3)
H(5a)	0.473(2)	0.537(3)	–0.230(3)	0.055(7)
H(5b)	0.570(2)	0.499(3)	–0.184(3)	0.053(7)
H(6a)	0.4154(17)	0.172(4)	–0.008(2)	0.053(7)
H(6b)	0.3872(19)	0.232(4)	–0.117(2)	0.060(8)
H(7a)	–0.1428(19)	–0.035(4)	–0.204(3)	0.060(8)
H(7b)	–0.115(17)	0.159(4)	–0.198(2)	0.058(7)
H(8a)	0.1168(17)	0.073(4)	–0.132(2)	0.055(6)
H(8b)	0.1389(17)	0.208(4)	–0.044(2)	0.052(6)
H(9a)	0.325(2)	0.069(4)	0.133(3)	0.073(8)
H(9b)	0.3516(17)	–0.093(4)	0.086(2)	0.058(7)
H(10a)	0.3007(18)	0.592(4)	–0.046(2)	0.058(6)
H(10b)	0.3335(18)	0.721(4)	–0.125(2)	0.070(8)
H(11a)	0.0744(18)	–0.365(4)	–0.043(2)	0.057(7)
H(11b)	–0.008(2)	–0.359(4)	–0.120(3)	0.076(9)
x = 0.97				
Cu(1)	–½	½	½	0.01936(5)
Cu(2)	0	1.0	½	0.01811(5)
S(1)	–0.4863(1)	0.7863(1)	0.1262(1)	0.01670(6)
O(1)	–0.3174(2)	0.4265(1)	0.3484(2)	0.0280(2)
O(2)	–0.4561(2)	0.8015(1)	–0.1148(2)	0.0250(2)
O(3)	–0.0338(2)	0.9066(1)	0.7971(2)	0.0311(2)
O(4)	–0.0651(2)	0.6245(1)	1.1287(2)	0.0295(2)
O(5)	–0.5915(2)	0.6518(1)	0.1745(2)	0.0262(2)
O(6)	–0.2107(2)	0.6171(1)	0.6492(2)	0.0262(2)
O(7)	–0.2551(2)	0.8177(1)	0.2972(2)	0.0270(2)
O(8)	–0.2544(2)	1.0837(1)	0.4806(2)	0.0343(2)
O(9)	–0.6399(2)	0.8723(1)	0.1374(2)	0.0273(2)
H(1)	–0.336(4)	1.101(2)	0.373(4)	0.044(5)
H(2)	–0.145(4)	0.8861(19)	0.825(3)	0.041(5)
H(3)	–0.174(4)	0.619(2)	0.790(4)	0.063(7)
H(4)	–0.233(3)	0.4765(19)	0.280(3)	0.040(5)
H(5)	0.083(4)	0.902(2)	0.909(4)	0.049(6)
H(6)	0.069(4)	0.629(2)	0.157(4)	0.057(6)
H(7)	–0.374(4)	0.376(2)	0.275(4)	0.047(6)
H(8)	–0.284(3)	0.0931(18)	0.590(4)	0.035(5)
H(9)	–0.080(4)	0.689(2)	1.197(4)	0.054(6)
H(10)	–0.198(4)	0.686(2)	0.581(4)	0.065(7)
x = 1.00				
Cu(1)	–½	½	½	0.01858(5)
Cu(2)	0	1.0	½	0.01742(5)
S(1)	–0.4869(1)	0.7864(1)	0.1253(1)	0.01575(6)
O(1)	–0.3177(2)	0.4268(1)	0.3484(2)	0.0271(2)
O(2)	–0.4559(2)	0.8016(1)	–0.1153(2)	0.0240(2)
O(3)	–0.0341(2)	0.9067(1)	0.7967(2)	0.0303(3)
O(4)	–0.0659(2)	0.6245(1)	1.1277(2)	0.0285(2)
O(5)	–0.5925(2)	0.6518(1)	0.1730(2)	0.0251(2)
O(6)	–0.2113(2)	0.6172(1)	0.6483(2)	0.0252(2)
O(7)	–0.2557(2)	0.8174(1)	0.2965(2)	0.0259(2)
O(8)	–0.2542(2)	1.0833(1)	0.4808(2)	0.0335(3)
O(9)	–0.6404(2)	0.8724(1)	0.1368(2)	0.0260(2)
H(1)	–0.340(3)	1.1006(17)	0.370(3)	0.028(4)
H(2)	–0.146(4)	0.886(2)	0.823(4)	0.050(6)
H(3)	–0.185(3)	0.6187(19)	0.786(4)	0.045(6)
H(4)	–0.233(3)	0.4776(17)	0.280(3)	0.029(4)
H(5)	0.094(4)	0.899(2)	0.916(4)	0.050(6)
H(6)	0.073(4)	0.628(2)	1.162(4)	0.050(6)
H(7)	–0.375(3)	0.3718(19)	0.272(3)	0.033(5)
H(8)	–0.285(3)	1.092(2)	0.576(4)	0.040(6)
H(9)	–0.078(4)	0.689(2)	1.194(4)	0.046(6)
H(10)	–0.196(5)	0.688(3)	0.578(5)	0.086(9)

TABLE 4A. Selected structural and distortional parameters for ($Co_{1-x}Cu_x$)SO_4·7H_2O

xCu	0.00	0.03	0.07	0.12	0.18	0.25	0.35	0.46
M(1)-O8 (Å) x2	2.033(1)	2.031(1)	2.030(1)	2.028(1)	2.027(1)	2.025(1)	2.020(1)	2.017(1)
M(1)-O7 (Å) x2	2.104(1)	2.104(1)	2.102(1)	2.101(1)	2.100(1)	2.101(1)	2.097(1)	2.099(1)
M(1)-O11 (Å) x2	2.112(1)	2.114(1)	2.115(1)	2.114(1)	2.119(1)	2.117(1)	2.124(1)	2.124(1)
<M(1)-O> (Å)	2.083	2.083	2.082	2.081	2.082	2.081	2.080	2.080
Volume (Å³)	11.988	11.993	11.980	11.959	11.979	11.966	11.951	11.941
BLD* M(1) (%)	1.60	1.67	1.68	1.71	1.76	1.80	1.94	2.01
ELD† M(1) (%)	2.26	2.21	2.19	2.19	2.23	2.19	2.26	2.23
OAV‡ M(1)(°)	10.82	9.89	9.70	9.47	9.50	9.23	9.13	8.78
QOE§ M(1)	1.0036	1.0034	1.0034	1.0033	1.0034	1.0033	1.0035	1.0034
κ|| M(1)	0.964	0.963	0.963	0.962	0.961	0.960	0.957	0.955
M(2)-O5 (Å) x2	2.059(2)	2.052(1)	2.050(1)	2.045(1)	2.037(1)	2.029(1)	2.019(1)	2.001(1)
M(2)-O6 (Å) x2	2.076(2)	2.066(1)	2.059(1)	2.056(1)	2.046(1)	2.037(1)	2.025(1)	2.003(1)
M(2)-O10 (Å) x2	2.136(2)	2.155(1)	2.166(1)	2.173(1)	2.189(1)	2.215(1)	2.241(1)	2.296(1)
<M(2)-O> (Å)	2.091	2.091	2.092	2.091	2.091	2.093	2.095	2.100
Volume (Å³)	12.170	12.173	12.168	12.173	12.158	12.194	12.209	12.265
BLD M(2) (%)	1.45	2.05	2.37	2.59	3.14	3.86	4.65	6.23
ELD M(2) (%)	1.11	1.30	1.79	1.51	1.71	1.97	2.38	3.21
OAV M(2)(°)	1.97	1.71	1.76	1.71	1.62	1.57	1.50	1.53
QOE M(2)	1.0011	1.0014	1.0018	1.0020	1.0027	1.0038	1.0052	1.0090
κ M(2)	1.033	1.047	1.054	1.059	1.072	1.090	1.108	1.147
S-O4 (Å)	1.462(1)	1.465(1)	1.465(1)	1.465(1)	1.465(1)	1.466(1)	1.466(1)	1.466(1)
S-O2 (Å)	1.470(1)	1.473(1)	1.473(1)	1.471(1)	1.472(1)	1.473(1)	1.474(1)	1.475(1)
S-O3 (Å)	1.480(1)	1.477(1)	1.475(1)	1.476(1)	1.476(1)	1.477(1)	1.476(1)	1.477(1)
S-O1 (Å)	1.481(1)	1.481(1)	1.479(1)	1.477(1)	1.478(1)	1.479(1)	1.477(1)	1.478(1)
<S-O> (Å)	1.473	1.474	1.473	1.472	1.473	1.474	1.473	1.474
Volume (Å³)	1.644	1.643	1.640	1.638	1.639	1.643	1.640	1.643
BLD (%)	0.50	0.34	0.28	0.30	0.29	0.28	0.25	0.26
TAV# (°)	0.32	0.47	0.40	0.42	0.43	0.51	0.42	0.43
TQE**	1.0001	1.0001	1.0001	1.0001	1.0001	1.0001	1.0001	1.0001

Abbreviations:

* $BLD = \frac{100}{n}\sum_{i=1}^{n}\frac{\left|(X-O)_i - (<X-O>)\right|}{(<X-O>)}$ %, *n* = amount of cation – anion bonds and X-O = cation – anion (oxygen) distance (Renner and Lehmann 1986);

† $ELD = \frac{100}{n}\sum_{i=1}^{n}\frac{\left|(O-O)_i - (<O-O>)\right|}{(<O-O>)}$ %, *n* = amount of edges and (O – O) = oxygen – oxygen interatomic distance defining an edge of the octahedron (Renner and Lehmann 1986);

‡ $OAV = \sigma^2_{\theta(oct)} = \sum_{i=1}^{12}(\Theta_i - 90°)^2 / 11$ with Θ_i = O-M-O bonding angle (Robinson et al 1971);

§ $OQE = \left\langle \lambda_{oct} \right\rangle = \sum_{i=1}^{6}\frac{\left(l_i/l_o\right)^2}{6}$ (Robinson et al 1971);

|| κ = average of the equatorial M-O bond lengths/average of the apex M-O bond lengths;

\# $TAV = \sigma^2_{\theta(tet)} = \sum_{i=1}^{6}(\Theta_i - 109.57°)^2 / 5$ with Θ_i = O-T-O bonding angle (Robinson et al 1971);

** $TQE = \left\langle \lambda_{tet} \right\rangle = \sum_{i=1}^{4}\frac{\left(l_i/l_o\right)^2}{4}$ (Robinson et al 1971).

Individual and average S-O bond lengths are almost unaltered by the substitution of Co^{2+} by Cu^{2+} (Table 4, Fig. 5) and the values found here are very similar to those reported in literature (Kellerson et al. 1991; Baur 1964a).

Table 5 summarizes information on water molecules and hydrogen bonding for the ($Co_{1-x}Cu_x$)SO_4·7H_2O series. While all oxygen atoms donate hydrogen bonds to neighboring M1, M2 octahedra, and the sulfate tetrahedron, the O10 oxygen atom is the only one that also accepts a hydrogen bond. This is interpreted in Kellerson et al. (1991) to be the reason for the elongation of the M2-O10 bond in $CoSO_4$·7D_2O. The elongation of the M2 polyhedron due to this threefold hydrogen bonding obviously makes the M2 site more adapted for Cu^{2+} (with its distinctly anisotropic coordination chemistry resulting from the $3d^9$-electric configuration) than the M1 site. Within the ($Co_{1-x}Cu_x$)SO_4·7H_2O series largest changes in hydrogen bonding can be found for the bonds donated by the free water molecule. Here the bond to the sulfate tetrahedron (O9-H2···O2) increases by 0.018(2) Å, while the bond to the O10 oxygen atom of the M(2)$(H_2O)_6$ octahedron is enhanced and decreases by as much as 0.134(2) Å. It was discussed in Kellerson et al. (1991) that the hydrogen bond O9-H7 might be bifurcated with O10 and the O4 oxygen atom of the sulfate tetrahedron. Actually the O9-H7···O10 and the O9-H7···O4 hydrogen bonds are both large and of similar size in the Co-rich part of the solid-solution series (Table 5). However, with increasing Cu^{2+} content the bond length to the O10 oxygen is shortened while the O4 atom successively moves further away [3.088(2) Å in $Co_{0.54}Cu_{0.46}SO_4$·7H_2O]. We conclude that toward the Cu^{2+} -rich compositions the bifurcation of the O9-H7 hydrogen bond is successively removed.

TABLE 4B. Selected structural and distortional parameters for ($Co_{1-x}Cu_x$)SO_4·5H_2O

xCu	0.97	1.00
M(1)-O1 (Å) x2	1.965(1)	1.960(1)
M(1)-O6 (Å) x2	1.972(1)	1.967(1)
M(1)-O5 (Å) x2	2.370(1)	2.380(1)
<M(1)-O> (Å)	2.102	2.103
Volume (Å³)	12.229	12.224
BLD* M(1) (%)	8.49	8.80
ELD† M(1) (%)	4.43	4.60
OAV‡ M(1)(°)	2.97	2.83
QOE§ M(1)	1.0169	1.0180
κ|| M(1)	1.204	1.212
M(2)-O8 (Å) x2	1.927(1)	1.923(1)
M(2)-O3 (Å) x2	1.957(1)	1.956(1)
M(2)-O7 (Å) x2	2.427(1)	2.431(1)
<M(2)-O> (Å)	2.104	2.103
Volume (Å³)	12.173	12.163
BLD M(2) (%)	10.25	10.38
ELD M(2) (%)	5.37	5.45
OAV M(2)(°)	5.23	5.22
QOE M(2)	1.0249	1.0255
κ M(2)	1.250	1.253
S-O9 (Å)	1.472(1)	1.472(1)
S-O5 (Å)	1.472(1)	1.473(1)
S-O7 (Å)	1.476(1)	1.475(1)
S-O2 (Å)	1.489(1)	1.484(1)
<S-O> (Å)	1.476	1.476
Volume (Å³)	1.650	1.650
BLD (%)	0.30	0.28
TAV# (°)	1.04	1.11
TQE**	1.0002	1.0003

Note: Abbreviations as in Table 4a.

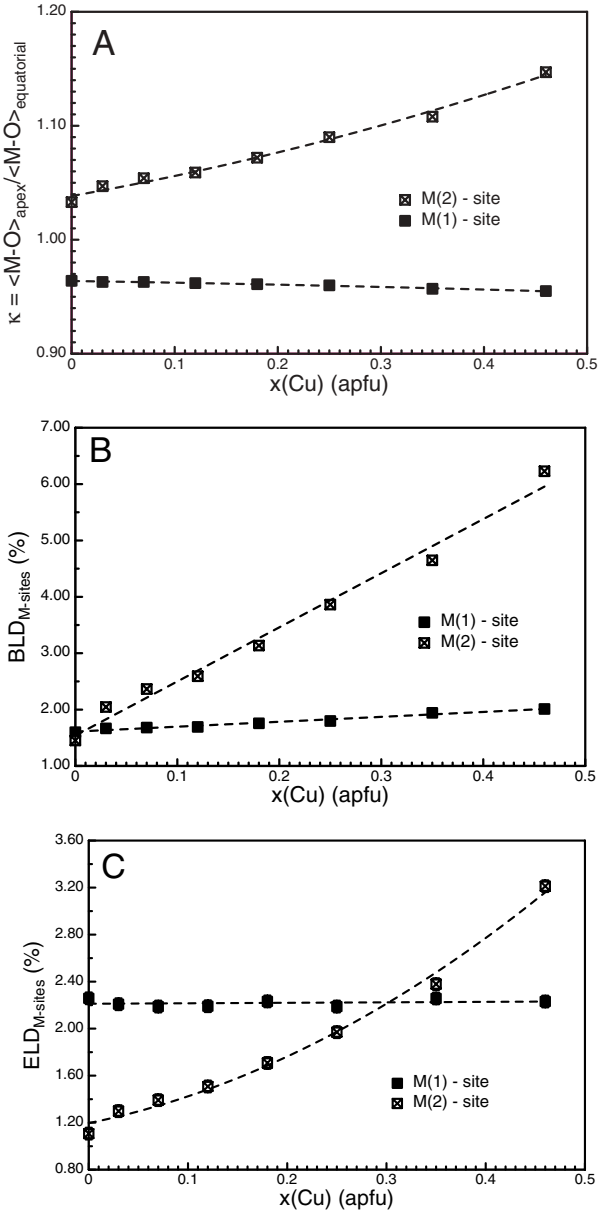

FIGURE 4. Octahedral distortion parameters of the M2 site as compared to the M1 octahedron for the synthetic samples along the ($Co_{1-x}Cu_x$)SO_4·7H_2O solid-solution series; second-order polynomial functions have been fitted to the data.

Optical spectroscopy

The optical spectra of the hepta-hydrate solid-solution compounds show signatures of both the Cu^{2+} and the Co^{2+} absorptions (Figs. 6a–6d). The well-developed and sharp absorption features between 26 300 and 16 700 cm^{-1} in the spectrum of $Co_{0.93}Cu_{0.07}SO4·7H_2O$ (Fig. 6a) and the broad band ranging from 10 500 to ~7150 cm^{-1} can be ascribed to spin-allowed d-d transitions of Co^{2+} in an octahedral crystal field, while the weak band centered at 12 500 cm^{-1} is due to Cu^{2+}. Bands below 7150 cm^{-1} are assigned to the first overtone and combination modes of H_2O stretching and bending vibrations. With increasing Cu^{2+} substitution the weak Cu^{2+} band evolves to a broad asymmetric absorption contribution ranging from 16 670 to ~9090 cm^{-1}, overlapping with the broad Co^{2+} band at 8330 cm^{-1} (Fig. 6b). Pure end-member chalcantite (Fig. 6c) exhibits just the broad asymmetric Cu^{2+} absorption contributions. In addition to the dominating Cu^{2+} absorption, sample $Co_{0.03}Cu_{0.97}SO_4·5H_2O$ shows a very weak band at 22 420 cm^{-1}, which is the signature and the proof of its small Co^{2+} content (inset in Fig. 6c).

The Co^{2+} contribution

Assuming O_h symmetry as a first approximation, the broad intense band in $Co_{0.97}Cu_{0.07}SO_4·7H_2O$ at 8490 cm^{-1} can be ascribed to a $^4T_{1g}$ (^4F) → $^4T_{2g}$ (^4F) transition. In $K_2Co_2(SeO_3)_3$ this transition is reported at 6880 cm^{-1} (with a shoulder at 7700 cm^{-1}) (Wildner and Langer 1994), in $CoSO_4·H_2O$ it is observed around 7500 cm^{-1} (Wildner 1996) and in erythrite $Co_3(AsO_4)_2·8H_2O$ at 7400 and 8200 cm^{-1} depending on orientation (Faye and Nickel 1968). The shift of the transition toward higher wavenumbers correlates well with decreasing average Co-O bond lengths in these compounds [viz. $K_2Co_2(SeO_3)_3$ with <Co-O> = 2.123 Å, Wildner and Langer 1994; $CoSO_4·H_2O$ with <Co-O> = 2.092 Å, Wildner 1996; and $Co_{0.97}Cu_{0.07}SO_4·7H_2O$ with <Co-O> = 2.083(1) and 2.091(1) Å]. The shoulder at 16 530 cm^{-1} in $Co_{0.97}Cu_{0.07}SO_4·7H_2O$ (Fig. 6a) is assigned to the $^4T_{1g}$ (^4F) → $^4A_{2g}$ (^4F) transition. The low intensity of this band is ascribed to the fact that it arises from a two-electron transition ($t^5_{2g}e^2_g$ → $t^3_{2g}e_g{}^4$) that has a much lower transition probability (Marfunin 1979; Taran and Rossman 2001; Ulrich et al. 2004). The prominent band system centered at ~20 000 cm^{-1} originates from the $^4T_{1g}$ (^4F) → $^4T_{2g}$ (^4P) transition. The appearance of several overlapping bands instead of a single one

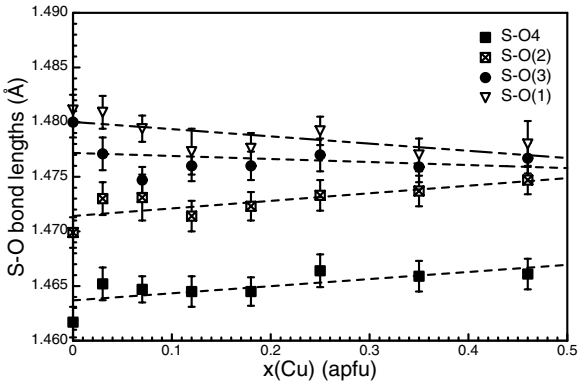

FIGURE 5. Variation of individual S-O bond lengths along the $(Co_{1-x}Cu_x)SO_4·7H_2O$ solid-solution series; linear regression lines have been fitted to the data.

implies that the actual symmetry at the Co^{2+} site is lower than O_h thus lifting degeneracy and producing the observed splitting (e.g., Marfunin 1979; Wildner 1996; Ulrich et al. 2004).

The metal cations in the hepta-hydrate series occupy the crystallographic 2*a* and 2*e* positions, both with site symmetry $\bar{1}$ (C_i), however, D_{4h} symmetry can be assumed in a good approximation (tetragonal bi-pyramids). In a tetragonal crystal field, the $^4T_{2g}$ (F) term is split into ^4E_g and $^4B_{2g}$, the $^4A_{2g}$ term transforms to $^4B_{1g}$ and the $^4T_{1g}$ (F, P) term splits into $^4A_{2g}$ and ^4E_g (Ulrich et al. 2004). Assuming ^4E_g (F) as the ground state, 5 bands may be expected in the spectral range covered here. Furthermore, in Co^{2+}-rich samples, two different crystallographic sites M1 and M2 are occupied. From Figure 6a ($Co_{0.93}Cu_{0.07}SO_4·7H_2O$) it is evident that the band centered at 8500 cm^{-1} is broad. We assume that it arises from at least two overlapping components (centered at 9094 and 8149 cm^{-1}; Table 6), which can be assigned to transitions to the ^4E_g (F) and $^4B_{2g}$ (F) terms.

The prominent band system at ~20 000 cm^{-1} can be deconvoluted into five bands, three of them being intense (Fig. 7a). The three main bands are assigned to the $^4A_{2g}$ (P) and ^4E_g (P) transitions of Co^{2+} on M1 and M2 positions. In sample $Co_{0.54}Cu_{0.46}SO_4·7H_2O$ (Fig. 7b), the splitting of this 20 000 cm^{-1} band system is less complex. De-convolution into Gaussian components shows two main bands at 21 173 and 19 150 cm^{-1} and a very weak band at 25 878 cm^{-1}. Additional bands, added to the refinement converged toward zero intensity and vanished. As it is reasonable to assume that Co^{2+} almost exclusively occupies the M1 site in sample $Co_{0.54}Cu_{0.46}SO_4·7H_2O$, the latter weak band is assigned to a spin-forbidden transition of Co^{2+} on M1, while the two former ones are ascribed to $^4A_{2g}$ (P) and ^4E_g (P) transitions at the M1 site. In analogy, bands at 22 305 and 19 228 cm^{-1} in $Co_{0.93}Cu_{0.07}SO_4·7H_2O$ are ascribed to the M1 site, while the band at 20 643 cm^{-1} probably arises from a $^4A_{2g}$ (P) and/or ^4E_g (P) transitions of Co^{2+} at the M2 site. The lower complexity of the Co^{2+} absorptions in $Co_{0.54}Cu_{0.46}SO_4·7H_2O$ is further evidence for the ordering of Co^{2+} and Cu^{2+} onto M1 and M2, respectively.

The Cu^{2+} contribution

Analytical de-convolution of the chalcantite absorption spectra into Gaussian components exhibit three main bands. Assuming a tetragonal crystal field (4+2-fold coordination) these bands can be assigned to the $^2B_{1g} \rightarrow {}^2B_{2g}$ (D_{4h}) transition (9699 cm^{-1}), to the $^2B_{1g} \rightarrow {}^2A_{1g}$ (D_{4h}) transition (11 860 cm^{-1}) and the $^2B_{1g} \rightarrow {}^2E_g$ (D_{4h}) transitions (13 308 cm^{-1}). Schematic energy level diagrams for Cu^{2+} including transition energies for $CuSO_4·5H_2O$ and $Co_{0.54}Cu_{0.46}SO_4·7H_2O$ are given in Figure 8. From the proposed band assignment, the splitting of the ^2E_g term (O_h symmetry) in chalcantite amounts to ~11 415 cm^{-1} (1.415 eV), suggesting that Cu^{2+} is in a strongly elongated octahedron with tetragonal symmetry, not far from a square planar coordination, while the splitting of the $^2T_{2g}$ level (O_h symmetry) is 3800 cm^{-1} (0.471 eV). Following Lakshman and Reddy (1973) and Marfunin (1979) the tetragonal splitting parameters D_s and D_t calculate as –2173 and –545 cm^{-1}, respectively, values that are slightly smaller than those given in Lakshman and Reddy (1973). The spectrum of the Co^{2+} substituted chalcantite $Cu_{0.97}Co_{0.03}SO_4·5H_2O$ closely resembles the appearance of the chalcantite spectrum (Table 6, Fig. 6c).

For the sample $Co_{0.54}Cu_{0.46}SO_4·7H_2O$ the Cu^{2+} high-energy band at 13 752 cm^{-1} is again ascribed to the $^2B_{1g} \rightarrow {}^2E_g$ transition. However, as the tetragonal distortion of the Cu-containing M2 site is smaller in the hepta-hydrate than in pure $CuSO_4·5H_2O$ (Fig. 5a), it is straightforward to assume that the term splitting decreases also. For this reason the low-energy band at 10 298 cm^{-1} is now ascribed to the $^2B_{1g} \rightarrow {}^2A_{1g}$ transition instead of $^2B_{1g} \rightarrow {}^2B_{2g}$ as in pure chalcantite (Table 6, Fig. 8b). Using this band assignment, the splitting of the $^2T_{2g}$ term (O_h symmetry) is reduced to ~1255 cm^{-1} (0.156 eV), while the ^2E_g term (O_h symmetry) is split by 10 300 cm^{-1} (1.277 eV). Both values are smaller in comparison with pure chalcantite, consistent with the expectation from the structural data and term diagrams (Marfunin 1979). As bond length variations clearly show a decreasing tetragonal elongation with decreasing Cu^{2+} content, one has to expect a decreasing splitting of $^2T_{2g}$ and ^2E_g terms within a D_{4h} field. Calculation of the parameters D_s and D_t give –1651 and –739 cm^{-1}, respectively.

Other oxidic compounds containing Cu-Co

To check for compounds with similar Cu^{2+}-Co^{2+} ordering schemes as found in the bieberite series, the "Inorganic Crystal Structure Database" (ICSD) was consulted. Indeed several compounds were found containing both transition metal cations. Among the most frequently occurring material in the ICSD is $YBa_2Cu_3O_{7-\delta}$ with some replacement of Cu by Co. Wu et al. (1998) reported that among the two Cu positions 1*a* and 2*g* of tetragonal $YBa_2Cu_{2.82}Co_{0.17}O_{6.54}$ (space group *P*4/*mmm*) Co with a valence of +2 prefers the 1*a* position while no Co enters the 2*g* position. The 1*a* position is sixfold-coordinated with Cu-O bonds of 1.840 Å (×2) and 1.938 Å (×4), thus representing a slightly compressed octahedron, while the 2*g* position has 4 oxygen atoms at a distance of 1.953 Å and one at a long distance of 2.398 Å. From this it is not surprising that Co enters the 1*a* position. A very similar ordering scheme was found by Voronin et al. (2000), Kajitani et al. (1987, 1988) for $YBa_2Cu_2CoO_{7.16}$. In this composition, the 1*a* position is almost completely filled by Co^{2+}, while Cu^{2+} resides on the 2*g* position, meaning that Co^{2+} prefers the compressed octahedral site similar to bieberite solid solution and does not enter the 4+1-fold coordinated 2*g* site.

Petrov et al. (1989) investigated the cationic distribution in

TABLE 5. Water molecules and hydrogen bonding in synthetic $Co_{1-x}Cu_xSO_4 \cdot nH_2O$ compounds

Donor	H	Acceptor	D-H (Å)	H···A (Å)	D···A (Å)	D-H···A (°)
$CoSO_4 \cdot 7H_2O$, x = 0.00						
O(5)	--H(5a)	..O(9)	0.90(5)	1.83(5)	2.713(4)	168(4)
O(5)	--H(5b)	..O(4)	0.71(4)	2.13(4)	2.798(3)	158(5)
O(6)	--H(6b)	..O(2)	0.87(5)	2.11(5)	2.963(4)	170(5)
O(6)	--H(6a)	..O(9)	0.69(6)	2.10(6)	2.731(4)	152(6)
O(7)	--H(7a)	..O(2)	0.95(6)	1.94(5)	2.866(3)	167(5)
O(7)	--H(7b)	..O(3)	0.74(5)	2.05(5)	2.782(3)	168(6)
O(8)	--H(8a)	..O(1)	0.59(4)	2.20(4)	2.750(3)	155(5)
O(9)	--H(9b)	..O(10)	0.62(5)	2.59(6)	3.029(4)	131(7)
O(10)	--H(10a)	..O(1)	0.76(4)	2.09(4)	2.843(3)	169(4)
O(10)	--H(10b)	..O(4)	0.76(4)	2.02(4)	2.772(4)	177(5)
O(11)	--H(11a)	..O(1)	0.70(4)	2.19(4)	2.881(3)	170(5)
O(11)	--H(11b)	..O(3)	0.99(5)	1.97(5)	2.952(3)	170(4)
$Co_{0.97}Cu_{0.03}SO_4 \cdot 7H_2O$, x = 0.03						
O(5)	--H(5a)	..O(9)	0.77(2)	1.94(2)	2.7109(17)	179(3)
O(5)	--H(5b)	..O(4)	0.75(2)	2.04(2)	2.7872(16)	172.5(17)
O(6)	--H(6a)	..O(9)	0.81(2)	1.92(2)	2.7260(16)	174(2)
O(6)	--H(6b)	..O(2)	0.84(2)	2.12(2)	2.9517(15)	175(2)
O(7)	--H(7a)	..O(2)	0.80(2)	2.08(2)	2.8686(16)	167.0(19)
O(7)	--H(7b)	..O(3)	0.801(19)	1.99(2)	2.7832(16)	169.8(19)
O(8)	--H(8a)	..O(3)	0.76(2)	1.97(2)	2.7266(16)	178(2)
O(8)	--H(8b)	..O(1)	0.77(2)	1.98(2)	2.7420(16)	171(2)
O(9)	--H(9a)	..O(2)	0.81(3)	2.00(3)	2.7803(15)	164(2)
O(9)	--H(9b)	..O(10)	0.79(3)	2.34(2)	3.0033(15)	142(2)
O(9)	--H(9b)	..O(4)	0.79(3)	2.49(2)	3.0152(15)	125.5(19)
O(10)	--H(10a)	..O(1)	0.82(2)	2.03(2)	2.8369(14)	165.2(19)
O(10)	--H(10b)	..O(4)	0.82(2)	1.96(2)	2.7735(14)	173(2)
O(11)	--H(11a)	..O(1)	0.81(2)	2.065(19)	2.8758(15)	177.3(19)
O(11)	--H(11b)	..O(3)	0.81(2)	2.17(2)	2.9590(15)	166(2)
$Co_{0.93}Cu_{0.07}SO_4$ * 7 H_2O, x = 0.07						
O(5)	--H(5a)	..O(9)	0.77(2)	1.95(2)	2.7120(19)	178.2(11)
O(5)	--H(5b)	..O(4)	0.79(3)	2.00(3)	2.7847(18)	173(3)
O(6)	--H(6a)	..O(9)	0.75(2)	1.98(2)	2.7264(19)	172(3)
O(6)	--H(6b)	..O(2)	0.83(3)	2.13(3)	2.9545(18)	173(3)
O(7)	--H(7a)	..O(2)	0.83(3)	2.06(3)	2.8688(18)	166(2)
O(7)	--H(7b)	..O(3)	0.80(3)	1.99(3)	2.7809(18)	171(2)
O(8)	--H(8a)	..O(3)	0.75(2)	1.98(2)	2.7269(19)	174(2)
O(8)	--H(8b)	..O(1)	0.76(3)	1.99(2)	2.7412(18)	171(2)
O(9)	--H(9a)	..O(2)	0.83(3)	1.99(3)	2.7810(18)	160(3)
O(9)	--H(9b)	..O(10)	0.73(3)	2.41(2)	2.9969(19)	140(2)
O(9)	--H(9b)	..O(4)	0.73(3)	2.52(2)	3.0198(18)	128(2)
O(10)	--H(10a)	..O(1)	0.83(3)	2.02(3)	2.8336(17)	166(2)
O(10)	--H(10b)	..O(4)	0.84(2)	1.94(2)	2.7723(17)	175(3)
O(11)	--H(11a)	..O(1)	0.83(2)	2.05(2)	2.8764(18)	176.0(19)
O(11)	--H(11b)	..O(3)	0.81(2)	2.16(2)	2.9639(18)	169(2)
$Co_{0.88}Cu_{0.12}SO_4 \cdot 7H_2O$, x = 0.12						
O(5)	--H(5a)	..O(9)	0.78(3)	1.94(3)	2.711(2)	176(3)
O(5)	--H(5b)	..O(4)	0.79(3)	2.00(3)	2.787(2)	177(3)
O(6)	--H(6a)	..O(9)	0.77(2)	1.96(2)	2.725(2)	176(3)
O(6)	--H(6b)	..O(2)	0.78(2)	2.18(2)	2.956(2)	177(2)
O(7)	--H(7a)	..O(2)	0.77(3)	2.11(3)	2.8702(17)	169(2)
O(7)	--H(7b)	..O(3)	0.82(3)	1.97(3)	2.7803(18)	170(2)
O(8)	--H(8a)	..O(3)	0.74(2)	1.99(2)	2.728(2)	174(2)
O(8)	--H(8b)	..O(1)	0.77(3)	1.98(2)	2.740(2)	169(2)
O(9)	--H(9a)	..O(2)	0.80(3)	2.02(3)	2.7818(19)	161(3)
O(9)	--H(9b)	..O(10)	0.74(3)	2.38(2)	2.995(2)	142(2)
O(9)	--H(9b)	..O(4)	0.74(3)	2.52(2)	3.0228(18)	126(2)
O(10)	--H(10a)	..O(1)	0.85(3)	2.01(3)	2.8323(17)	163(2)
O(10)	--H(10b)	..O(4)	0.82(2)	1.95(2)	2.7668(17)	175(2)
O(11)	--H(11a)	..O(1)	0.81(2)	2.07(2)	2.8772(19)	177(2)
O(11)	--H(11b)	..O(3)	0.79(2)	2.19(3)	2.9639(19)	168(3)
$Co_{0.82}Cu_{0.18}SO_4 \cdot 7H_2O$, x = 0.18						
O(5)	--H(5a)	..O(9)	0.74(2)	1.97(2)	2.709(2)	179(3)
O(5)	--H(5b)	..O(4)	0.79(3)	1.99(3)	2.781(2)	176(2)
O(6)	--H(6a)	..O(9)	0.73(2)	2.00(2)	2.722(2)	175(3)
O(6)	--H(6b)	..O(2)	0.79(3)	2.17(3)	2.951(2)	175(3)
O(7)	--H(7a)	..O(2)	0.87(3)	2.02(3)	2.865(2)	164(3)
O(7)	--H(7b)	..O(3)	0.80(3)	1.99(3)	2.783(2)	172(2)
O(8)	--H(8a)	..O(3)	0.75(2)	1.98(2)	2.720(2)	176.2(18)
O(8)	--H(8b)	..O(1)	0.75(2)	1.99(2)	2.737(2)	172(2)
O(9)	--H(9a)	..O(2)	0.73(3)	2.08(3)	2.7876(19)	162(3)
O(9)	--H(9b)	..O(10)	0.76(3)	2.33(2)	2.976(2)	144(2)
O(9)	--H(9b)	..O(4)	0.76(3)	2.54(2)	3.0346(19)	125(2)
O(10)	--H(10a)	..O(1)	0.82(2)	2.03(2)	2.8320(19)	166(2)
O(10)	--H(10b)	..O(4)	0.81(2)	1.96(2)	2.7667(19)	175(2)
O(11)	--H(11a)	..O(1)	0.86(2)	2.01(2)	2.8745(19)	177(2)
O(11)	--H(11b)	..O(3)	0.76(3)	2.22(3)	2.9669(18)	165(3)
$Co_{0.75}Cu_{0.15}SO_4 \cdot 7H_2O$, x = 0.25						
O(5)	--H(5a)	..O(9)	0.77(3)	1.93(3)	2.7043(19)	177(3)
O(5)	--H(5b)	..O(4)	0.77(3)	2.01(3)	2.7772(18)	174(2)
O(6)	--H(6a)	..O(9)	0.80(2)	1.92(2)	2.7201(19)	175(2)
O(6)	--H(6b)	..O(2)	0.76(2)	2.19(2)	2.9500(17)	173(3)
O(7)	--H(7a)	..O(2)	0.83(3)	2.05(3)	2.8631(18)	166(2)
O(7)	--H(7b)	..O(3)	0.79(3)	2.00(3)	2.7829(18)	172(2)
O(8)	--H(8a)	..O(3)	0.76(2)	1.96(2)	2.7180(19)	173(2)
O(8)	--H(8b)	..O(1)	0.78(3)	1.96(3)	2.7318(18)	171(2)
O(9)	--H(9a)	..O(2)	0.82(3)	2.00(3)	2.7868(18)	161(2)
O(9)	--H(9b)	..O(10)	0.74(3)	2.31(2)	2.9577(18)	147(2)
O(9)	--H(9b)	..O(4)	0.74(3)	2.58(2)	3.0442(17)	123(2)
O(10)	--H(10a)	..O(1)	0.85(3)	2.00(3)	2.8292(17)	165(2)
O(10)	--H(10b)	..O(4)	0.81(2)	1.97(2)	2.7663(17)	171(2)
O(11)	--H(11a)	..O(1)	0.83(2)	2.05(2)	2.8774(18)	176.6(17)
O(11)	--H(11b)	..O(3)	0.79(2)	2.21(3)	2.9696(18)	162(3)
$Co_{0.65}Cu_{0.35}SO_4 \cdot 7H_2O$, x = 0.35						
O(5)	--H(7a)	..O(9)	0.75(2)	1.95(2)	2.703(2)	179(3)
O(5)	--H(8b)	..O(4)	0.83(3)	1.95(3)	2.7705(18)	174(2)
O(6)	--H(6a)	..O(9)	0.73(2)	1.99(2)	2.718(2)	174(3)
O(6)	--H(8a)	..O(2)	0.76(3)	2.19(3)	2.9466(19)	175(3)
O(7)	--H(6b)	..O(2)	0.86(3)	2.03(3)	2.8617(19)	164(3)
O(7)	--H(5b)	..O(3)	0.81(3)	1.98(3)	2.7841(18)	173(2)
O(8)	--H(9b)	..O(3)	0.78(2)	1.94(2)	2.715(2)	175(2)
O(8)	--H(5a)	..O(1)	0.77(3)	1.97(3)	2.729(2)	170(2)
O(9)	--H(9a)	..O(2)	0.76(3)	2.07(3)	2.7931(19)	158(3)
O(9)	--H(9b)	..O(10)	0.73(3)	2.28(2)	2.9351(19)	150(2)
O(10)	--H(10a)	..O(1)	0.82(3)	2.03(3)	2.8291(19)	164(2)
O(10)	--H(10b)	..O(4)	0.80(2)	1.98(2)	2.7666(17)	169(2)
O(11)	--H(11a)	..O(1)	0.84(2)	2.04(2)	2.8802(19)	175(2)
O(11)	--H(11b)	..O(3)	0.80(3)	2.20(3)	2.9749(19)	164(3)
$Co_{0.54}Cu_{0.46}SO_4 \cdot 7H_2O$, x = 0.46						
O(5)	--H(7a)	..O(9)	0.77(3)	1.94(3)	2.7037(19)	172(3)
O(5)	--H(8b)	..O(4)	0.83(3)	1.93(3)	2.7600(19)	174(3)
O(6)	--H(6a)	..O(9)	0.77(2)	1.95(2)	2.714(2)	177(2)
O(6)	--H(8a)	..O(2)	0.75(2)	2.19(2)	2.9406(18)	175(3)
O(7)	--H(6b)	..O(2)	0.79(3)	2.08(3)	2.8548(19)	169(3)
O(7)	--H(5b)	..O(3)	0.81(3)	1.98(3)	2.7831(18)	172(2)
O(8)	--H(9b)	..O(3)	0.78(2)	1.93(2)	2.707(2)	174(2)
O(8)	--H(5a)	..O(1)	0.75(3)	1.98(3)	2.722(2)	171(2)
O(9)	--H(9a)	..O(2)	0.80(3)	2.03(3)	2.7985(18)	161(3)
O(9)	--H(9b)	..O(10)	0.74(3)	2.22(2)	2.8950(19)	151(2)
O(10)	--H(10a)	..O(1)	0.85(3)	2.00(3)	2.8228(19)	162(2)
O(10)	--H(10b)	..O(4)	0.82(2)	1.95(2)	2.7616(18)	171(2)
O(11)	--H(11a)	..O(1)	0.79(3)	2.09(3)	2.8818(19)	175(2)
O(11)	--H(11b)	..O(3)	0.77(3)	2.25(3)	2.9865(19)	160(3)
$CuSO_4 \cdot 5H_2O$						
O(8)	--H(1)	..O(2)	0.741(18)	1.995(18)	2.7108(15)	162.5(19)
O(3)	--H(2)	..O(2)	0.73(3)	2.03(2)	2.7521(15)	171(2)
O(6)	--H(3)	..O(4)	0.79(2)	1.95(2)	2.7338(15)	171(2)
O(1)	--H(4)	..O(4)	0.821(18)	1.952(18)	2.7611(16)	168.2(19)
O(3)	--H(5)	..O(9)	0.90(2)	1.81(2)	2.7056(15)	174(2)
O(4)	--H(6)	..O(5)	0.81(3)	1.99(3)	2.7790(15)	167(2)
O(1)	--H(7)	..O(2)	0.750(19)	2.107(19)	2.8476(15)	169.5(18)
O(8)	--H(8)	..O(9)	0.67(2)	2.00(2)	2.6692(15)	176(3)
O(4)	--H(9)	..O(7)	0.86(2)	2.18(2)	2.9865(15)	157(2)
O(6)	--H(10)	..O(7)	0.81(3)	2.03(3)	2.7908(14)	156(3)
$Cu_{0.97}Co_{0.03}SO_4 \cdot 5H_2O$						
O(8)	--H(1)	..O(2)	0.72(2)	2.01(2)	2.7073(14)	163(2)
O(3)	--H(2)	..O(2)	0.73(2)	2.04(2)	2.7568(15)	171(2)
O(6)	--H(3)	..O(4)	0.80(2)	1.93(2)	2.7348(14)	176(3)
O(1)	--H(4)	..O(4)	0.816(19)	1.958(19)	2.7607(15)	168(2)
O(3)	--H(5)	..O(9)	0.83(2)	1.89(2)	2.7070(14)	171(2)
O(4)	--H(6)	..O(5)	0.79(3)	2.00(3)	2.7811(15)	171(2)
O(1)	--H(7)	..O(2)	0.70(2)	2.15(2)	2.8462(14)	169(2)
O(8)	--H(8)	..O(9)	0.75(2)	1.92(2)	2.6691(14)	177(2)
O(4)	--H(9)	..O(7)	0.88(2)	2.16(2)	2.9901(15)	158(2)
O(6)	--H(10)	..O(7)	0.79(2)	2.05(2)	2.7914(14)	156(2)

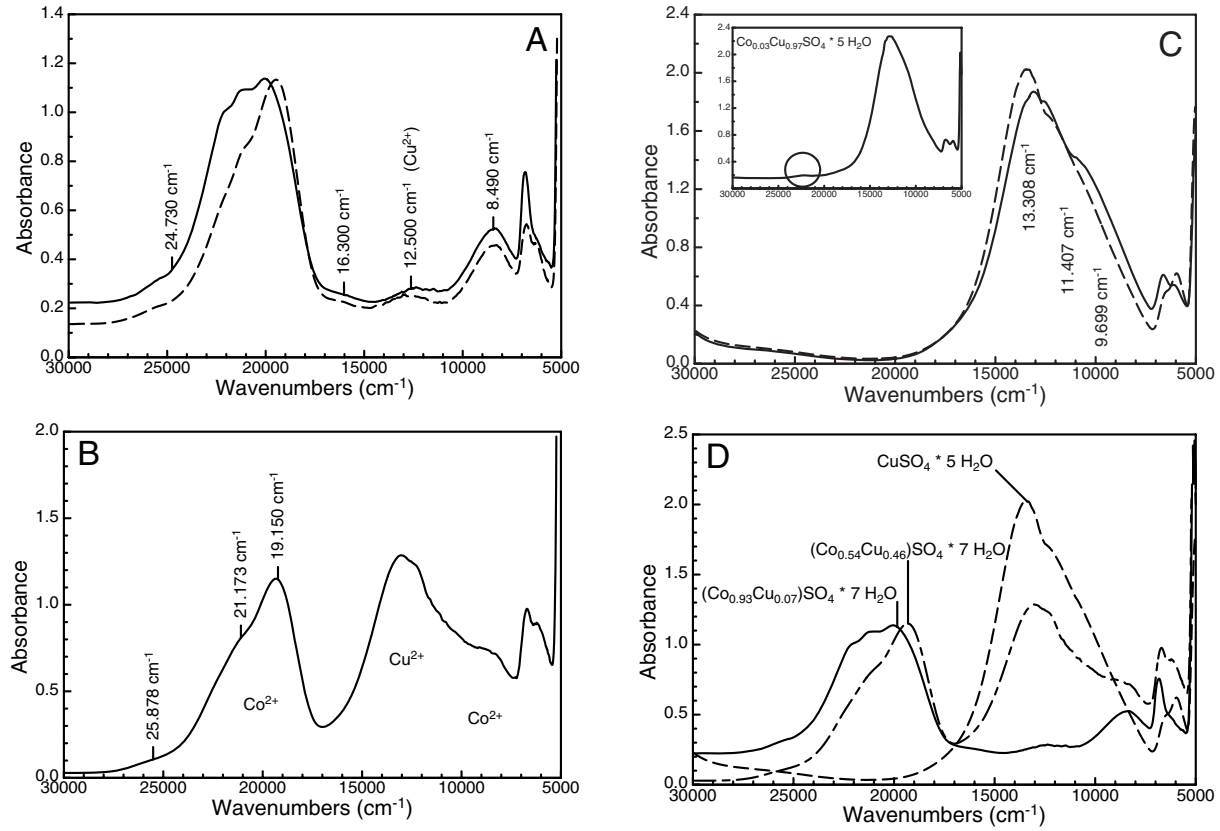

FIGURE 6. Optical absorption spectra of (**a**) $Co_{0.97}Cu_{0.07}SO_4·7H_2O$, (**b**) $Co_{0.54}Cu_{0.46}SO_4·7H_2O$, (**c**) $CuSO_4·5H_2O$. (**d**) Comparisons of spectra shown in **a**–**c**. Solid and broken lines in **a** and **c** represent two different dark-field orientations.

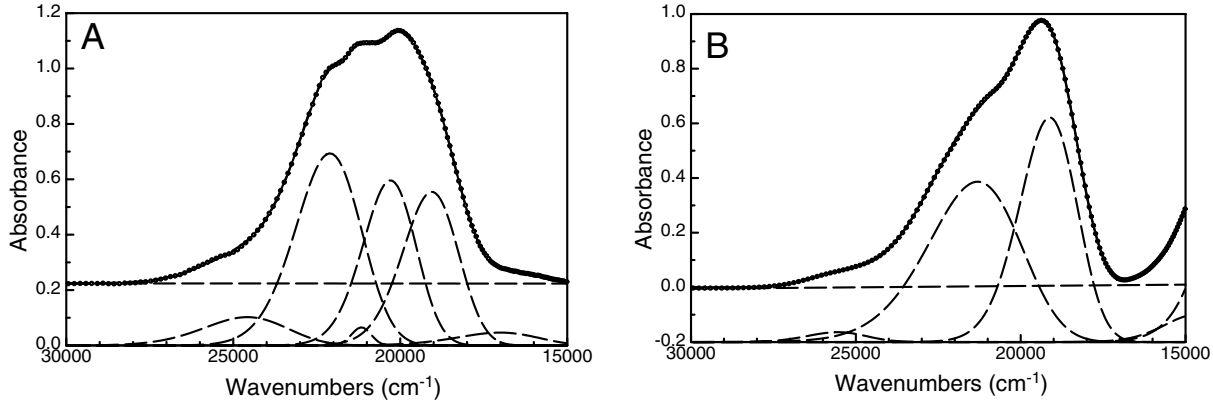

FIGURE 7. Gaussian curve fitting of the Co^{2+} $^4T_{1g}$ (^4F) → $^4T_{2g}$ (^4P) transition (O_h symmetry) for sample $Co_{0.93}Cu_{0.07}SO_4·7H_2O$ (**a**) and for sample $Co_{0.54}Cu_{0.46}SO_4·7H_2O$ (**b**).

cubic $Fd\bar{3}m$ $Cu_xCo_{3-x}O_4$ spinels. Here it was found that Cu^{2+} incorporation mainly takes place at the fourfold-coordinated 8*a*-site, while only minor Cu^{2+} replaces Co^{3+} at the sixfold-coordinated site. For a composition of $Cu_{0.95}Co_{2.05}O_4$ Petrov et al. (1989) report bond lengths (Cu,Co)-O = 1.919 Å (×4) for the 8*a* and (Cu,Co)-O = 1.946 Å (×4) and 1.919 Å (×2) for the 16*d* position. This implies that Co prefers the tetragonally compressed octahedral site, similar to the bieberite series. Hohlwein et al. (1989) investigated structural changes in the superconducting $La_{1.8}Sr_{0.2}Cu_{1-x}Co_xO_4$ system ($0 \le x \le 0.5$), space group *I*4/*mmm*. Only one distinct site is present here for the transition metals. In the pure end-member compound $La_{1.8}Sr_{0.2}CuO_4$ the Cu-O bond lengths are 1.887 Å (×4) and 2.409 Å (×2), the 2*a*-site thus can be described as a distinctly elongated octahedron. Incorporation of Co^{2+} into this compound, requires that this substitution take place on the 2a position, resulting in significant changes in transition

TABLE 6. Results of Gaussian component analysis of optical absorption spectra of $Co_{1-x}Cu_xSO_4$·nH_2O compounds with proposed band assignment in D_{4h} symmetry

λ (nm)*	Γ (cm^{-1})†	ν (cm^{-1})†	Assignment
$CuSO_4$·5H_2O (α), x = 1.00			
656	3887	15234	Cu^{2+}
741	2660	13308	Cu^{2+} $^2B_1 \rightarrow {}^2E_g$ (D_{4h})
876	2238	11407	Cu^{2+} $^2B_1 \rightarrow {}^2A_{1g}$ (D_{4h})
1031	2778	9699	Cu^{2+} $^2B_1 \rightarrow {}^2B_{2g}$ (D_{4h})
1527	435	6547	H_2O
1681	597	5949	H_2O
$CuSO_4$·5H_2O (β); x = 1.00			
642	3613	15567	Cu^{2+}
741	2756	13488	Cu^{2+} $^2B_1 \rightarrow {}^2E_g$
843	3473	11860	Cu^{2+} $^2B_1 \rightarrow {}^2A_{1g}$
1027	2867	9735	Cu^{2+} $^2B_1 \rightarrow {}^2B_{2g}$
1499	428	6670	H_2O
1640	813	6097	H_2O
$Cu_{0.97}Co_{0.03}SO_4$·5H_2O			
445	1319	22466	Co^{2+} $^4A_{2g}$ (P), ^4E_g (P)
668	3740	14968	Cu^{2+}
766	3068	13060	Cu^{2+} $^2B_1 \rightarrow {}^2E_g$
903	2373	11071	Cu^{2+} $^2B_1 \rightarrow {}^2A_{1g}$
1076	2792	9340	Cu^{2+} $^2B_1 \rightarrow {}^2B_{2g}$
1500	586	6667	H_2O
1674	512	5974	H_2O
1945	170	5141	H_2O
2330	167	4291	H_2O
$Cu_{0.46}Co_{0.54}SO_4$·7H_2O			
386	3598	25878	Co^{2+} (M1) spin-forbidden
472	3129	21173	Co^{2+} (M1) $^4A_{2g}$ (P), ^4E_g (P)
522	1915	19150	Co^{2+} (M1) $^4A_{2g}$ (P), ^4E_g (P)
727	2664	13752	Cu^{2+} $^2B_1 \rightarrow {}^2E_g$
800	2642	12508	Cu^{2+} $^2B_1 \rightarrow {}^2B_{2g}$
971	2325	10298	Cu^{2+} $^2B_1 \rightarrow {}^2A_{1g}$
1143	1184	8748	Co^{2+} (M1) $^4A_{2g}$ (F), ^4E_g (F)
1237	638	8083	Co^{2+} (M1) $^4A_{2g}$ (F), ^4E_g (F)
1478	440	6764	H_2O
1617	807	6182	H_2O
$Cu_{0.07}Co_{0.93}SO_4$·7H_2O (α)			
441	3364	24304	Co^{2+} (M1) spin-forbidden
448	2274	22305	Co^{2+} (M1) $^4A_{2g}$ (P), ^4E_g (P)
470	495	21241	Co^{2+} (M2) spin-forbidden
484	2491	20643	Co^{2+} (M2) $^4A_{2g}$ (P), ^4E_g (P)
520	2264	19228	Co^{2+} (M1) $^4A_{2g}$ (P), ^4E_g (P)
615	1668	16252	Co^{2+} (M1+M2) $^4B_{1g}$
795	1935	12580	Cu^{2+} $^2B_1 \rightarrow {}^2E_g$
903	2948	11080	Cu^{2+} $^2B_1 \rightarrow {}^2B_{2g}$
1099	1637	9094	Co^{2+} (M1+M2) $^4A_{2g}$ (F), ^4E_g (F)
1227	1181	8149	Co^{2+} (M1+M2) $^4A_{2g}$ (F), ^4E_g (F)
1462	402	6839	H_2O
1567	780	6380	H_2O
1966	495	5085	H_2O
$Cu_{0.07}Co_{0.93}SO_4$·7H_2O (β)			
405	3042	24730	Co^{2+} (M1) spin-forbidden
445	2192	22487	Co^{2+} (M1) $^4A_{2g}$ (P), ^4E_g (P)
476	2003	20996	Co^{2+} (M2) spin-forbidden
513	1742	19498	Co^{2+} (M2) $^4A_{2g}$ (P), ^4E_g (P)
538	1492	18558	Co^{2+} (M1) $^4A_{2g}$ (P), ^4E_g (P)
594	2302	16823	Co^{2+} (M1+M2) $^4B_{1g}$
751	1503	13325	Cu^{2+} $^2B_1 \rightarrow {}^2E_g$
800	1492	12495	Cu^{2+} $^2B_1 \rightarrow {}^2B_{2g}$
1125	1461	8890	Co^{2+} (M1+M2) $^4A_{2g}$ (F), ^4E_g (F)
1245	1845	8035	Co^{2+} (M1+M2) $^4A_{2g}$ (F), ^4E_g (F)
1467	465	6813	H_2O
1595	716	6267	H_2O
1972	562	5072	H_2O

Notes: λ = band position in wavelength, Γ = full width at half maximum of Gaussian band, ν = band position in transition energy; * = band position calculated from wavenumber values, † = values from numeric peak fitting.

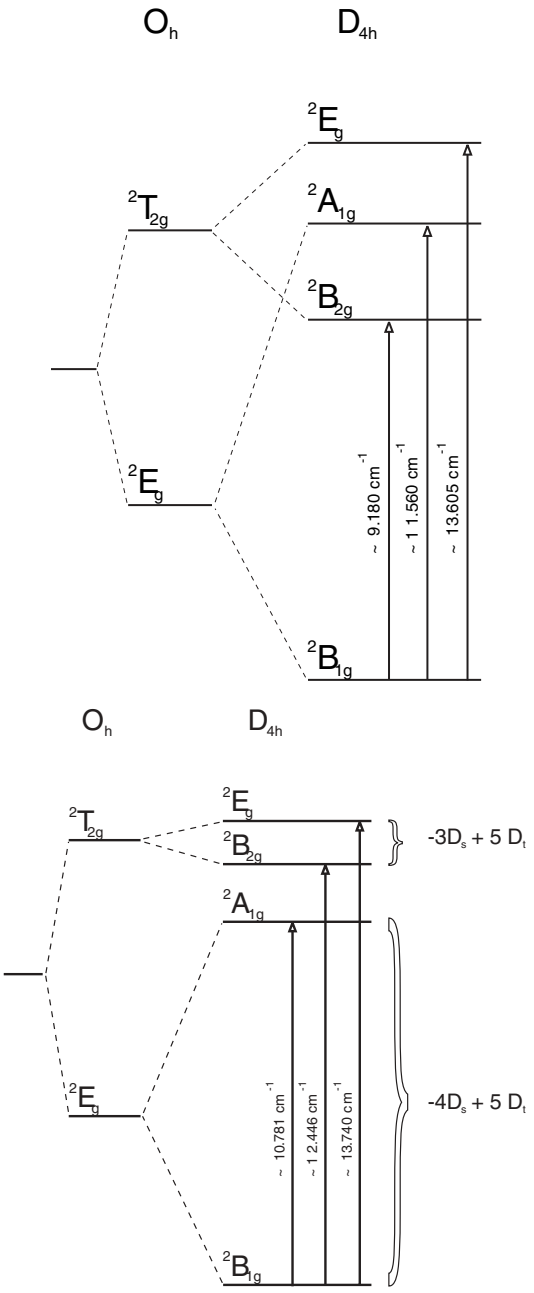

FIGURE 8. Schematic energy term diagrams for Cu^{2+} in elongated octahedral crystal fields (tetragonal elongation); splitting scheme as proposed for (**a**) pure $CuSO_4$·5H_2O and for (**b**) $Co_{0.54}Cu_{0.46}SO_4$·7H_2O.

metal bond lengths (M-O). This mainly affects the two long M-O bonds, which decrease to 2.374 Å for a replacement of only x = 0.1 Cu^{2+} by Co^{2+}. For the composition $La_{1.8}Sr_{0.2}Cu_{0.4}Co_{0.5}O_4$ bond lengths are 1.910 Å (×4) and 2.220 Å (×2). For x = 0.0 the tetrahedral elongation κ = 1.277, which decreases to κ = 1.162 for x = 0.5. From these data it can be concluded that the behavior of the 2*a* site in $La_{1.8}Sr_{0.2}Cu_{1-x}Co_xO_4$ is similar to that of the M2 site in the bieberite solid-solution series.

Besides compounds with Co-Cu substitution on one and the

same site, others are known where the two transition metals are found on distinct sites. Among them, Müller-Buschbaum and Tomaszewska (1991) report on the orthorhombic structure of $CoCu_2O_3$ (space group *Pmmn*). Here Co^{2+} is found on the sixfold-coordinated 2*a* position with bond lengths of 2.013, 2.144, and 2.250 Å (each 2×), while Cu^{2+} occupies the 4*f* position with Cu-O bond lengths of 1.945 (×2), 2.000 (×2), 2.548, and 2.705 Å. The Co-site can be described as a compressed octahedron while the Cu-site is a 4+2 fold coordinated site as it is typical for Cu^{2+}. $KCo_3Cu(As_{2.58}V_{0.42})O_{12}$, space group *C*2/*c*, which was studied by Frerichs and Müller-Buschbaum (1994), has three distinct sites for the transition metal cations. Cu^{2+} again is found on the fourfold-coordinated site (Cu-O = 1.919 Å and 1.947 Å); Co^{2+} resides on sixfold-coordinated sites. However, one of the Co^{2+} sites (4*e*) is tetragonally elongated with Co-O bond lengths of 2.108, 2.112, and 2.180 Å, while the second one (8*f*-site) again can be described as tetragonally compressed.

Acknowledgments

G.J.R. thanks the Austrian Fonds zur Förderung der wissenschaftlichen Forschung (FWF) for financial support under grant R33-N10. The manuscript benefited much from critical and thorough reviews of Michail Taran, Richard Thompson, and AE Eugen Libowitzky; their help is acknowledged very much.

References cited

Bacon, G.E. and Titterton, D.H. (1975) Neutron diffraction studies of $CuSO_4$·5 H_2O and $CuSO_4$·5D_2O. Zeitschrift für Kristallographie, 141, 330–341.

Baur, W.H. (1964a) On the crystal chemistry of salt hydrates. III. The determination of the crystal structure of $FeSO_4$·7 H_2O (melanterite). Acta Crystallographica, 17, 1167–1174.

——— (1964b) On the crystal chemistry of salt hydrates. IV. The refinement of the crystal structure of $MgSO_4$·7 H_2O (epsomite). Acta Crystallographica, 17, 1361

Benabbas, A. (2006) Review of polyhedral distortions as a multi-scale minimization of the electric polarization and their correlation with physical properties. Acta Crystallographica, B62, 9–15.

Brandenburg, K. and Putz, H. (2005) Diamond 3.0d: Crystal and Molecular Structure Visualization Program, Crystal-Impact, K. Brandenburg and H. Putz GbR, Postfach 1251, D-53002 Bonn, Germany.

Burns, P.C. and Hawthorne, F.C. (1996) Static and dynamic Jahn-Teller effects in Cu^{2+} oxysalt minerals. Canadian Mineralogist, 34, 1089–1105.

Calleri, M., Cavetti, A., Ivaldi, G., and Rubbo M. (1984) Synthetic epsomite, $MgSO_4$·7H_2O: absolute configuration and surface features of the complementary (111) forms. Acta Crystallographica, B40, 218–222.

Collins, E.M. and Menzies, A.W.C. (1936) A comparative method for measuring aqueous vapour and dissociation pressures with some of its applications. Journal of Applied Crystallography, 40, 379–397.

Farrugia, L.J. (1999) WinGX suite for small-molecule single-crystal crystallography. Journal of Applied Crystallography, 32, 837–838.

Faye, G.H. and Nickel, E.H. (1968) The origin of pleochroism in erythrite. Canadian Mineralogist, 9, 493–504.

Frerichs, D. and Müller-Buschbaum, H. (1994) Ein Beitrag zur Kristallchemie von Verbindungen mit Johilleritstruktur: $KCo_3Cu(As_{2.58}V_{0.42})O_{12}$. Zeitschrift für Naturforschung, Teil B, 49, 1463–1466.

Hawthorne, F.C., Krivovichev, S.V., and Burns, P.C. (2000) Crystal chemistry of sulfate minerals. In C.N. Alpers, J.L. Jambor, and D.K. Nordstrom, Eds, Sulfate Minerals—Crystallography, Geochemistry and Environmental Significance, 40, p. 1–112. Reviews in Mineralogy and Geochemistry, Mineralogical Society of America, Chantilly, Virginia.

Hohlwein, D., Hoser, A., Sonntag, R., Prandl, W., Schäfer, W., Kieml, R., Kemmler-Sach, S., and Hewat, A.W. (1989) Structural changes in superconducting $La_{1.8}Sr_{0.2}CuO_4$ by alloying copper with cobalt. Physik (Berlin), 156, 893–896.

Iskhakova, L.D., Dubrovinskii, L.S., and Charushnikova, I. (1991) Crystal structure, calculation of parameters of atomic interaction potential and thermochemical properties of $NiSO_4$·nH_2O (n = 6, 7). Kristallografiya, 36, 650–655 (in Russian).

Kajitani, T., Kusaba, K., Kikuchi, M., Syono, Y., and Hirabayashi, M. (1987) Crystal structure of tetragonal $YBa_2Cu_{3-d}Co_dO_{7-g}$ (d = 0.0, 0.3). Japanese Journal of Applied Physics, Part 2, 26, 1727–1730.

——— (1988) Crystal structures of $YBa_2Cu_{2-s}A_sO_{9-g}$ (A = Ni, Zn and Co). Japanese Journal of Applied Physics, Part 2, 27, 354–357.

Kellerson, T., Delaplane, R., and Olovsson, I. (1991) Disorder of a trigonally planar coordinated water molecule in cobalt sulphate heptahydrate, $CoSO_4$·7 H_2O (bieberite). Zeitschrift für Naturforschung, 46b, 1635–1640.

Lakshman, S.V.J. and Reddy, B.J. (1973) Optical absorption spectra of Cu^{2+} in chalcantite and malachite. Canadian Mineralogist, 12, 207–210.

Leverett, P., McKinnon, A.R., and Williams, P.A. (2004) New data for boothite, $CuSO_4$·7H_2O, from Burraga, New South Wales. Australian Journal of Mineralogy, 10, 3–6.

Marfunin, A.S. (1979) Physics of minerals and inorganic materials: an introduction. Springer-Verlag, New York.

Müller-Buschbaum, H. and Tomaszewska, A. (1991) Das erste Übergangsmetall-Oxocuprat (II) mit $CaCu_2O_3$-Struktur. Zur Kenntnis von $CoCu_2O_3$ und $Ca_{1-x}Co_xCu_2O_3$ (x = 0.55). Zeitschrift für Kristallographie 196, 121–127.

Peterson, R.C., Hammarstrom, J.M., and Robert, R.S. II (2006) Alpersite (Mg,Cu)SO_4·7H_2O, a new mineral of the melanterite group, and cuprian pentahydrite: Their occurrence within mine waste. American Mineralogist, 91, 261–269.

Petrov, K., Krezhov, K., and Konstantinov, P. (1989) Neutron diffraction study of the cationic distribution in $Cu_xCo_{3-x}O_4$ ($0 < x \leq 1.0$) spinels prepared by thermal decomposition of layered hydroxide nitrate precursors. Journal of Physics and Chemistry of Solids, 50, 577–581.

Renner, B. and Lehmann, G. (1986) Correlation of angular and bond lengths distortion in TO_4 units in crystals. Zeitschrift für Kristallographie, 175, 43–59.

Robinson, K., Gibbs, G.V., and Ribbe, P.H. (1971) Quadratic elongation, a quantitative measure of distortion in coordination polyhedra. Science, 172, 567–570.

Shannon, R.D. and Prewitt, C.T. (1969) Effective ionic radii in oxides and fluorides. Acta Crystallographica, B25, 925–934.

Sheldrick, G.M. (1997) SHELXS-97 and SHELXL-97: Programs for Crystal Structure Solution and Refinement. University of Göttingen, Germany.

Stoe and Cie (1996) X-SHAPE and X-RED: programs for optimizing of the crystal shape (w.r.t. the merging R-value) and numerical absorption correction. Stoe and Cie GmbH, Darmstadt, Germany.

Systat Software Inc. (1995) PeakFit 4.0 Program for analytical spectral refinement. Jandel Scientific Software, AISN Software Inc., San Raphael, California

Taran, M.N. and Rossmann, G.R. (2001) Optical spectra of Co^{2+} in three synthetic silicate minerals. American Mineralogist, 86, 889–895.

Ulrich, K., Ott, O., Langer, K., and Becker, K.D. (2004) Temperature dependence of the polarized electronic absorption spectra of olivines. Part II—Cobalt-containing olivines. Physics and Chemistry of Minerals, 31, 247–260.

Voronin, V.I., Goshchitskii, B.N., Mitberg, E., Leonidov, I.A., and Kozhevnikov, V.L. (2000) Valence state of cobalt atoms and crystal structure of $YBa_2Cu_{3-x}Co_xO_{6+\delta}$. Zhurnal Strukturnoi Khimii, 41(4), 626–631.

Waller, R. (1992) Temperature- and humidity-sensitive mineralogical and petrological specimen. In F.M. Howie, Ed., The care and conversation of geological material: Minerals, rocks, meteorites and lunar finds, p. 25–50. Elsevier, Oxford.

Wildner, M. (1996) Polarized electronic absorption spectra of Co^{2+} ions in the kieserite-type compounds $CoSO_4$·H_2O and $CoSeO_4$·H_2O. Physics and Chemistry of Minerals, 23, 489–496.

Wildner, M. and Langer, K. (1994) Co^{2+} in trigonal fields of oxygen based structures: Electronic absorption spectra of buetschliite-type $K_2Co(SeO_3)_2$, $K_2Co_2(SeO_3)_3$ and zemannite-type $K_2Co_2(SeO_3)_3$·2H_2O. Physics and Chemistry of Minerals, 20, 460–468.

Wilson, A.J.C., Ed. (1992) International Tables for Crystallography, Volume C. Kluwer Academic Publishers, Dordrecht.

Wu, X.S., Chen, W.M., Gou, C., Chen, D.F., and Sun, K. (1998) Neutron powder diffraction studies on $YBa_2Cu_3O_{7-\delta}$ with Co substitution. Diwen Wuli Xuebao, 20(2), 104–108.

Manuscript received February 3, 2006
Manuscript accepted November 6, 2006
Manuscript handled by Eugen Libowitzky